LIBRARY
ROYAL AIRCRAFT ESTABLISHMENT
BEDFORD.

This Document Provided by the Abbott Aerospace
TECHNICAL LIBRARY
ABBOTTAEROSPACE.COM

C.P. No. 1193

C.P. No. 1193

PROCUREMENT EXECUTIVE, MINISTRY OF DEFENCE

AERONAUTICAL RESEARCH COUNCIL

CURRENT PAPERS

Curvature Effects in the Diffraction of Short Waves into a Shadow

by

F. G. Leppington

Department of Mathematics, Imperial College

LONDON: HER MAJESTY'S STATIONERY OFFICE

1971

PRICE 77 *p* NET

This Document Provided by the Abbott Aerospace
Technical Library
abbottaerospace.com

THIS DOCUMENT PROVIDED BY THE ABBOTT AEROSPACE
TECHNICAL LIBRARY
ABBOTTAEROSPACE.COM

UDC 534.26 : 534-8

LIBRARY
ROYAL AIRCRAFT ESTABLISHMENT
BEDFORD.

C.P. No. 1193
October 1970†

CURVATURE EFFECTS IN THE DIFFRACTION OF SHORT WAVES INTO A SHADOW

by

F. G. Leppington*, Department of Mathematics, Imperial College

SUMMARY

PART A

The distant pressure field within the shadow cast by a point source in the presence of a semi-infinite rigid plane is compared with that for a rounded body. Within the 'deep shadow region', not too close to the shadow boundary, it is found that the field is much less for the rounded obstacle in the short wave limit, having exponentially small behaviour compared with the algebraic decay appropriate to the half-plane case. At points very close to the geometrical shadow boundary, on the other hand, the pressure field exhibits almost identical behaviour for each geometry, this being the familiar Fresnel pattern, but with a change of phase for the rounded body.

PART B

Consideration is given to the possibility of choosing the shape of a rounded obstacle, within certain overall restrictions, in order to minimise the diffracted field within the deep shadow region.

---

*Vacation Consultant (Summer 1970)
†Replaces RAE Technical Report 70183 - ARC 32505

THIS DOCUMENT PROVIDED BY THE ABBOTT AEROSPACE
TECHNICAL LIBRARY
ABBOTTAEROSPACE.COM

CONTENTS

PART A

GENERAL RESULTS ON DIFFRACTION BY SMOOTH BODIES

PART B

OPTIMISATION OF THE CURVATURE

THIS DOCUMENT PROVIDED BY THE ABBOTT AEROSPACE
TECHNICAL LIBRARY
ABBOTTAEROSPACE.COM

PART A

GENERAL RESULTS ON DIFFRACTION BY SMOOTH BODIES

1 INTRODUCTION

The elementary ray theory of optics and acoustics predicts zero field in the 'geometrical shadow region' that is cast by a scattering obstacle. The determination of short wave estimates for the small field that does propagate in such regions has attracted a great deal of attention in the literature, and it is found that the field is essentially different according as the scatterer has sharp or smooth edges.

Exact formal solutions have been obtained for relatively simple geometries such as semi-infinite plane, sphere, circular and parabolic cylinders, with a variety of boundary conditions prescribed, and these canonical solutions play a key role in developing and checking short wave theories for bodies of more general shape.

For smooth convex bodies, an extension of the ideas of ray theory has led Keller[1,2] to develop the concept of 'creeping waves' that propagate, from a source at P_o to an observer at a point P_1 in the shadow, along the shortest path $P_o Q_o Q_1 P_1$, where $P_o Q_o$ and $Q_1 P_1$ are tangents to the body and $Q_o Q_1$ is an arc thereon. According to this theory, energy decays by the inverse square law (or inverse linear law in two dimensions) along the straight sections $P_o Q_o$ and $Q_1 P_1$; it is argued that energy must decay more rapidly with arc length along the curved section $Q_o Q_1$ of the ray path, since energy is being constantly shed along tangents with a consequent exponential attenuation with arc length. Several plausible assumptions are made concerning the nature of the field along such a 'diffracted ray', and a comparison with exact solutions for the sphere (or circular cylinder in two dimensions) provides final details to yield an asymptotic estimate for the exponentially small field in the shadow, for the limit of waves of length very small compared with the typical radius of curvature of the body. The theory is not valid near the shadow boundary where a different sort of approximation is required.

One might anticipate that a sharp edge will provide a more efficient mechanism for scattering into a shadow, since a ray at incidence upon such an edge is expected to scatter in a more isotropic manner. This property is well established by the classical results of Sommerfeld, and MacDonald[3] for the semi-infinite plane, whence it is readily seen that the field is algebraically, rather than exponentially, small at high wave numbers.

THIS DOCUMENT PROVIDED BY THE ABBOTT AEROSPACE
TECHNICAL LIBRARY
ABBOTTAEROSPACE.COM

The object of the present Report is to compare the shadows cast by sharp and smooth ended bodies, with an observer at great distance from the scattering surface and with a source point relatively close to the body. For simplicity of exposition, attention is confined to twodimensional geometries, the acoustically hard boundary condition is taken, and the source and observation points lie in the same plane normal to the generators of the body. Generalisations from this twodimensional configuration and from this boundary condition are available, in principle, and several extensions are stated in the course of the analysis.

Within the 'deep shadow region', this excluding the immediate vicinity of the shadow boundary, a direct comparison is made between the results for a half-plane, and results for a rounded body calculated on the basis of Keller's theory[1] of creeping waves. It has already been mentioned that this theory is invalid in the 'shadow transition region' that separates shadow from illuminated regions. This transition region is treated at length in the literature, notably by Fock[4] whose results are interpreted in the present context in order to compare the transition zones for sharp and smooth bodies. The principal results obtained are that the field within an inner core of the transition region is nearly the same for both sharp and smooth edges, whereas the field within the deep shadow is considerably less for the smooth obstacle.

Time periodic oscillations are considered, whence the pressure fluctuation $P(\underline{x},t)$ in the sound field has the form

$$P(\underline{x},t) = \Re\{p(\underline{x}) \exp(-i\omega t)\} \quad , \tag{1-1}$$

where ω denotes the angular frequency; it is obvious that the time factor $e^{-i\omega t}$ will appear throughout and may therefore be dropped in the calculations that follow. The acoustic wave equation with harmonic time dependence takes the form

$$(\nabla^2 + k^2)\, p(\underline{x}) = 0 \quad , \tag{1-2}$$

where $k = \omega/c = 2\pi/\lambda$ is the radian wave number and λ the wavelength. Equation (1-2) has to be satisfied throughout the fluid, except for a source point $\underline{x} = \underline{x}_o$, together with the boundary condition

$$\partial p/\partial n = 0 \quad \text{on the scattering surface } S \quad , \tag{1-3}$$

THIS DOCUMENT PROVIDED BY THE ABBOTT AEROSPACE
TECHNICAL LIBRARY
ABBOTTAEROSPACE.COM

where n denotes the outward normal. Finally, in order to ensure outgoing waves at infinity, we require

$$p \sim F e^{ikr}/r \quad \text{or} \quad p \sim F e^{ikr}/r^{1/2} \quad \text{as} \quad r \to \infty \tag{1-4}$$

in three or two dimensions respectively, where r denotes the distance from some convenient origin.

2 THE RECIPROCAL THEOREM

If a point source is situated at a point $P_1(\underline{x}_1)$ with an observer measuring the pressure at a point $P_o(\underline{x}_o)$, then it is required to find the pressure induced by the source in the far field limit as $r_o = |\underline{x}_o| \to \infty$; and for the moment the points $\underline{x}_o$ and $\underline{x}_1$ are taken to lie in the same plane perpendicular to the generators of the twodimensional body. The far field limit $r_o \to \infty$ can be taken at an early stage in the calculations by appealing to the reciprocal theorem which states that the field at $\underline{x}_o$ due to a source at $\underline{x}_1$ is precisely the same as that at $\underline{x}_1$ due to a source at $\underline{x}_o$. Now in the limit $|\underline{x}_o| \to \infty$ it is clear that the incident field in this reciprocal problem becomes that of an incident plane wave of suitable amplitude and phase. Apart from the obvious desirability of taking the far field approximation at the outset of the calculations, there is the further advantage on account of the relative simplicity of plane wave against incident source field.

To formalise these ideas, suppose the incident field is that of a source given by

$$p_i = e^{ikR}/R \quad , \qquad R = |\underline{x}_1 - \underline{x}_o| \quad ; \tag{2-1}$$

then as $r_o = |\underline{x}_o| \to \infty$, with $\underline{x}_1$ fixed, we have

$$p_i \sim A e^{ik\underline{\alpha}.\underline{x}_1} = A e^{ik(x_1\cos\theta_o + y_1\sin\theta_o)} \quad , \tag{2-2}$$

where $A = e^{ikr_o}/r_o$ and $\underline{\alpha} = -\underline{x}_o/r_o$ is the unit vector in the direction from $\underline{x}_o$ towards the origin. Thus it remains to solve the reciprocal problem of a plane wave, given by (2-2), at incidence upon the obstacle, in terms of which the far field at $\underline{x}_o$ due to a source at $\underline{x}_1$ is given immediately.

In a similar way, the problem of finding the far field at $\underline{x}_o$ due to a line source at $\underline{x}_1$ can be reduced to that of an incident plane wave. Thus if

THIS DOCUMENT PROVIDED BY THE ABBOTT AEROSPACE TECHNICAL LIBRARY ABBOTTAEROSPACE.COM

$$p_1 = \left(\frac{\pi k}{2}\right)^{1/2} e^{i\pi/4} H_o^{(1)}(kR) \qquad (2\text{-}3)$$

where $H_o^{(1)}$ denotes a Hankel function, then in the limit $|\underline{x}_o| \to \infty$ we may use the asymptotic estimate

$$H_o^{(1)}(z) \sim \left(\frac{2}{\pi z}\right)^{1/2} e^{iz - i\pi/4} \quad \text{for large } z \qquad (2\text{-}4)$$

to find that

$$p_i \sim B\, e^{ik\underline{\alpha}.\underline{x}_1} \qquad (2\text{-}5)$$

where $B = e^{ikr_o}/r_o^{1/2}$ and $\underline{\alpha} = -\underline{x}_o/r_o$ as before.

Evidently the plane wave (2-5) differs from (2-2) only by its constant of proportionality; in particular, the ratio p/p_i of total pressure to incident pressure will be the same in each case. The consequence to be drawn from this property is that for calculating the ratio p/p_i in the far field, we may consider the incident field to be either a point source or line source or plane wave, as convenient.

3 THE RIGID HALF-PLANE

The problem of scattering by a rigid half-plane is a classical one whose solution is well known (MacDonald[3]), and can be written in several forms. Taking the incident field to be a plane wave given by

$$p_i(\underline{x}_1) = A \exp(ik\underline{\alpha} \cdot \underline{x}_1) = A \exp(ikr_1 \cos(\theta_1 - \theta_o)) \quad , \qquad (3\text{-}1)$$

where $\underline{\alpha}$ is the direction of incidence displayed in Fig.1, it is found that the total pressure distribution is given exactly by

$$p(\underline{x}) = A\,\pi^{-1/2}\, e^{ikr_1 - i\pi/4} \{F((2kr_1)^{1/2} \sin \tfrac{1}{2}(\theta_1 - \theta_o)) + F((2kr_1)^{1/2} \sin \tfrac{1}{2}(\theta_1 + \theta_o))\} \quad . \qquad (3\text{-}2)$$

In formula (3-2), F denotes the Fresnel integral

$$F(x) = e^{-ix^2} \int_x^\infty e^{it^2}\, dt \quad , \qquad (3\text{-}3)$$

THIS DOCUMENT PROVIDED BY THE ABBOTT AEROSPACE
TECHNICAL LIBRARY
ABBOTTAEROSPACE.COM

some properties of which are described in the appendix. The corresponding result for the soft half-plane, on which $p = 0$, differs from (3-2) only in the sign of the second Fresnel function.

According to the arguments of the preceding section, the ratio p/p_i gives immediately the ratio of total pressure against incident pressure at great distance $\underline{x}_o$ due to a point (or line) source at $\underline{x}_1$.

We are concerned here primarily with the 'geometrical shadow region', $\theta_o < \theta < \pi$, in most of which domain the ratio p/p_i is shown to be small for the short wave limit $kr_1 \gg 1$. In order to estimate p in this region, when $kr_1 \gg 1$, note that $\sin \frac{1}{2}(\theta_1 + \theta_o)$ is a positive number bounded away from zero, whence the argument $(2kr)^{1/2} \sin \frac{1}{2}(\theta_1 + \theta_o)$ is uniformly large, and F may be replaced by its asymptotic form (A-4) to get

$$F((2kr)^{1/2} \sin \tfrac{1}{2}(\theta_1 + \theta_o)) \sim -(2i(2kr)^{1/2} \sin \tfrac{1}{2}(\theta_1 + \theta_o))^{-1} .$$

A similar simplification can be effected for the other Fresnel function of formula (3-2), provided that $(\theta_1 - \theta_o)$ is not too small, i.e. for points $\underline{x}_1$ not too close to the shadow boundary. Specifically, if $(kr_1)^{1/2}(\theta_1 - \theta_o)$ is large, then the Fresnel integral may be simplified to get

$$\frac{p}{p_i} \sim \frac{\exp\{ikr_1(1 - \cos(\theta_1 - \theta_o)) + i\pi/4\}}{2\pi^{1/2}(2kr_1)^{1/2}} \{\operatorname{cosec} \tfrac{1}{2}(\theta_1 - \theta_o) + \operatorname{cosec} \tfrac{1}{2}(\theta_1 + \theta_o)\} , \quad (3\text{-}4)$$

for $(kr_1)^{1/2}(\theta_1 - \theta_o) \gg 1$, and this gives the ratio of far field against incident field due to a source at $\underline{x}_1$.

If θ_1 lies between $-\theta_o$ and $+\theta_o$, but not too close to either, then the first Fresnel integral may be replaced by its approximation (A-5) for large and negative argument, whence

$$p = A e^{ikr_1 \cos(\theta_1 - \theta_o)} + O(kr_1)^{-1/2} , \qquad kr_1 \gg 1 , \qquad (3\text{-}5)$$

and the field is almost the same as if there were no obstacle present. Similarly, it is easy to verify that the solution in the remaining region $-\pi < \theta_1 < \theta_o$ corresponds to the incident wave plus a reflected wave, when $kr_1 \gg 1$.

THIS DOCUMENT PROVIDED BY THE ABBOTT AEROSPACE TECHNICAL LIBRARY ABBOTTAEROSPACE.COM

In the shadow transition region, where θ_1 and θ_o are nearly equal, the first term of (3-2) varies rapidly to change the field from (3-4) to (3-5) within a small angle $\theta_1 - \theta_o = O(kr_1)^{-1/2}$, while the second term provides a relatively unimportant, slowly varying, background level. Thus

$$\frac{p}{p_i} = \pi^{-\frac{1}{2}} e^{2ikr_1(\theta_1-\theta_o)^2 - i\pi/4} F\left(\left(\frac{kr_1}{2}\right)^{1/2}(\theta_1 - \theta_o)\right) + O(kr_1)^{-1/2} . \quad (3\text{-}6)$$

It is readily seen that the same pattern obtains if the boundary condition changes to the soft one, $p = 0$, for it has already been remarked that the solution is then obtained by changing the sign of the second Fresnel integral of (3-2), whence (3-6) is altered only by changing the sign of the background sound field of order $(kr_1)^{-1/2}$.

This behaviour near the shadow boundary will be shown to appear in subsequent problems, even when the shape is smooth: the transition from shadow to illuminated zones is governed by a Fresnel integral of argument $(kt_1/2)^{1/2}(\theta_1 - \theta_o)$, (where t_1 denotes the length of ray path from $\underline{x}_1$ to the point of tangency on the body), superimposed upon a slowly varying background field. The real difference between the shadow formations due to sharp and smooth bodies arises in the deep shadow, not too close to the shadow boundary.

4 GEOMETRICAL DIFFRACTION IN THE DEEP SHADOW OF A CONVEX BODY

In order to contrast the shadow formations appropriate to sharp and smooth ended bodies, the present section concerns an asymptotic estimate for the field at P_o in the deep shadow of a source at P_1. The ratio p/p_i of far field against incident field has been shown in section 2 to be the same for either a point source or line source, and we here consider the latter force distribution, as a matter of convenience. For the sake of simplicity the curved end of the body is taken to have constant radius of curvature a, though there is no difficulty in extending the method to deal with bodies of continuously varying curvature. An asymptotic solution is sought in the short wave limit $\lambda \ll a$, whence $ka \gg 1$.

The required estimate is obtained by using the ideas due to Keller[1] of diffracted rays that feed energy into the shadow region shown in Fig.2. This analysis leads to an asymptotic estimate for the field at points in the deep shadow, not too close to the body or to the shadow boundary.

Following the procedure of section 2, the source and observation points are interchanged, by means of the reciprocal theorem, and the source point $\underline{x}_o$ is finally taken to be at large distance from the end, so that the incident

THIS DOCUMENT PROVIDED BY THE ABBOTT AEROSPACE
TECHNICAL LIBRARY
ABBOTTAEROSPACE.COM

field reduces to that of a plane wave. It is convenient to deal with a line source of incident field

$$p_i = B\left(\frac{\pi k}{2}\right)^{1/2} e^{i\pi/4} H_o^{(1)}(kR) \quad , \qquad R = |\underline{x}_1 - \underline{x}_o| \quad , \tag{4-1}$$

whence for large r_o we have from (2-5)

$$p_i \sim B \frac{e^{ikt_o}}{t_o^{1/2}} e^{ik\underline{\alpha}\cdot\underline{x}_1} \tag{4-2}$$

where $t_o = (r_o^2 - a^2)^{1/2}$ is the distance from P_o to the point of tangency Q_o.

Keller's theory of diffracted rays runs briefly as follows. Extending the elementary idea of propagation along rays in the illuminated region, it is postulated that energy is fed to a point P_1 in the shadow along a diffracted ray whose path length from P_o to P_1 is a minimum; that is, the ray has two straight sections $P_o Q_o$ and $Q_1 P_1$ that are tangents to the body, together with a curved section $Q_o Q_1$.

The decay of energy along the straight sections $P_o Q_o$ and $Q_1 P_1$ is controlled by energy considerations, demanding constant flux of energy along a narrow tube of rays; further, the phase is simply k times path length, this leading to the familiar expression

$$p \propto e^{ikt}/t^{1/2} \quad , \tag{4-3}$$

where t denotes distance along such a tangent, and expression (4-3) is replaced by e^{ikt}/t for threedimensional sources. Taking both straight sections into account we have

$$p \sim \Psi \frac{e^{ik(t_o+t_1)}}{(t_o\, t_1)^{1/2}} \tag{4-4}$$

where t_o and t_1 denote the lengths of $P_o Q_o$ and $Q_1 P_1$; $\Psi = \Psi(s';Q_o,Q_1)$ denotes the amplitude at s' of a ray that originates at Q_o and leaves the cylinder at Q_1, depends on the incident field, and has to account for the decay along the curved path $Q_o Q_1$. Formula (4-4) is obviously invalid when t_o (or t_1) becomes zero, since this corresponds to a point where rays meet, and a separate treatment is required.

THIS DOCUMENT PROVIDED BY THE ABBOTT AEROSPACE
TECHNICAL LIBRARY
ABBOTTAEROSPACE.COM

Some simple assumptions concerning the general form of the function Ψ, and an appeal to known results for a circular cylinder, now lead to its asymptotic evaluation for large ka. The rapidly varying phase term of Ψ is taken to be simply the wave number times path length, whence $\Psi = \psi\, e^{iks}$, where s is the arc length of $Q_o\, Q_1$. In order to ascertain the decay of Ψ with distance, it is noted that diffracted rays are shed in all tangential directions, and $Q_1\, P_1$ is but one of these rays (Fig.3).

It is certainly reasonable to conjecture that the energy shed at each intermediate station, arc length s' from Q_o, will be proportional to the energy at s', whence

$$\frac{d\psi}{ds'}(s';Q_o,Q_1) = -\alpha(s')\,\psi(s';Q_o,Q_1) \quad ,$$

i.e.
$$\psi(s;Q_o,Q_1) = \psi(0;Q_o,Q_1)\exp\left[-\int_o^s \alpha(s')\,ds'\right] . \qquad (4\text{-}5)$$

The decay rate is governed by the function $\alpha(s')$ of (4-5), and has to be found. Reciprocity between source and observation points implies that $\psi(0;Q_o,Q_1)$ is symmetrical with respect to Q_o and Q_1. Furthermore the <u>local nature</u> of the diffraction process, in the short wave limit, implies that waves are locally plane, whence $\alpha(s)$ is independent of the incident field and $\psi(0;Q_o,Q_1)$ depends on the incident field only through the constant B of the incident wave (4-2); the local nature of the diffraction process also implies that the positions Q_o and Q_1 have independent effects upon the value of ψ. All these requirements, for the short wave limit, imply the form

$$\psi(s;Q_o,Q_1) = B\, b(Q_o)\, b(Q_1)\exp\left[-\int_o^s \alpha(s')\,ds'\right] \quad , \qquad (4\text{-}6)$$

in which the two unknown functions $b(Q_o)$ and $\alpha(s)$ <u>depend only on the local geometry of the body</u>.

Collecting together the formulae ((4-4), (4-5), (4-6)), we have

$$p \sim B\,\frac{e^{ik(t_o+t_1+s)}}{(t_o\, t_1)^{1/2}}\, b(Q_o)\, b(Q_1)\exp\left[-\int_o^s \alpha(s')\,ds'\right] \quad . \qquad (4\text{-}7)$$

THIS DOCUMENT PROVIDED BY THE ABBOTT AEROSPACE
TECHNICAL LIBRARY
ABBOTTAEROSPACE.COM

The final stage of the calculation, the determination of b and α, is achieved by appealing to the exact solution for a given body, namely the circular cylinder. Since these diffraction coefficients depend only on the local geometry (i.e. curvature), such a calculation serves to determine b and α for more general shapes. Keller[2] shows that there is an infinite set of possible modes for b and α, given by

$$b_n^2 = \frac{1}{2\pi^{1/2}} \left(\frac{2\rho^2}{k}\right)^{1/6} e^{i\pi/12} \frac{1}{a_n \, Ai(a_n)^2} \tag{4-8}$$

and

$$\alpha_n = e^{-i\pi/6} \left(\frac{k}{2\rho^2}\right)^{1/3} a_n \tag{4-9}$$

in which $-a_n$ denote the (real negative) zeros of the Airy function Ai described in the appendix, and $\rho(s)$ denotes the radius of curvature at s. In the present case $\rho(s) = a$ = constant, and retaining only the leading term $n = 0$ in the expansion for large ka, we are led to the estimate that

$$p \sim B \frac{e^{ik(t_o+t_1+s)}}{(t_o \, t_1)^{1/2}} \frac{e^{i\pi/12}}{2\pi^{1/2}} \left(\frac{2a^2}{k}\right)^{1/6} \frac{1}{a_o \, Ai(a_o)^2} \exp\left(- a_o \, e^{-i\pi/6} \, (\tfrac{1}{2}ka)^{1/3} (\theta_1 - \theta_o)\right)$$

.... (4-10)

Greater accuracy can be obtained by adding higher terms in the expansion, using (4-8) and (4-9).

For bodies of continuously varying radius of curvature $\rho(s)$, one merely changes the factor $(2a^2/k)^{1/6}$ of (4-10) to $(2\rho(Q_1)\,\rho(Q_o)/k)^{1/6}$ and the exponential term $\exp\,(-\,a_o\,e^{-i\pi/6}\,(\tfrac{1}{2}ka)^{1/3}\,(\theta_1 - \theta_o)) =$ $\exp\,(-\,a_o\,e^{-i\pi/6}\,(k/2a^2)^{1/3}\,s)$ to $\exp\left(-\,a_o\,e^{-i\pi/6}\int_o^s (k/2\rho^2)^{1/3}\,ds\right)$.

In particular, for the far field approximation $r_o \to \infty$, we have $r_o \sim t_o$, whence the ratio of total to incident pressure distribution is given, with reference to (4-2) and (4-10) as

$$\left|\frac{p}{p_i}\right| \sim \frac{1}{2(\pi t_1)^{1/2}} \left(\frac{2a^2}{k}\right)^{1/6} \frac{1}{a_o \, A_i^2(a_o)} \exp\left(- a_o \frac{\sqrt{3}}{2} (\tfrac{1}{2}ka)^{1/3} (\theta_1 - \theta_o)\right)$$

THIS DOCUMENT PROVIDED BY THE ABBOTT AEROSPACE TECHNICAL LIBRARY ABBOTTAEROSPACE.COM

i.e.

$$\left|\frac{p}{p_i}\right| \sim 1.08 \frac{a^{1/3}}{k^{1/6}\, t_1^{1/2}} \exp\left(-0.700\ (ka)^{1/3}\ (\theta_1 - \theta_o)\right) \quad , \qquad (4\text{-}11)$$

$$ka \gg 1, \quad (ka)^{1/3}\ (\theta_1 - \theta_o) \gg 1 \quad .$$

This result should be compared with the corresponding one (3-4) for the shadow cast by a plate having a sharp edge. It is seen that (4-11) is exponentially small for the short wave limit, while (3-4) is but algebraically small. In particular, for points close to the shadow, $\theta_1 - \theta_o \ll 1$, but not too close, $(ka)^{1/3}\ (\theta - \theta_o) \gg 1$, a comparison of the shadow fields shows that

$$\left|\frac{p(\text{smooth body})}{p(\text{sharp body})}\right| \sim 1.53\ (ka)^{1/3}\ (\theta_1 - \theta_o) \exp\left(-0.700\ (ka)^{1/3}\ (\theta_1 - \theta_o)\right) \quad .... \quad (4\text{-}12)$$

which is of course small for $(ka)^{1/3}\ (\theta_1 - \theta_o) \gg 1$; thus the field is much smaller for the smooth ended body, even relatively close to the shadow boundary.

A separate analysis is required in the remaining transition region where $(ka)^{1/3}\ (\theta_1 - \theta_o) \lesssim 1$, in the vicinity of the geometrical shadow boundary, and this region is the subject of the next section.

5 THE TRANSITION REGION: $\theta_1 - \theta_o \lesssim (ka)^{-1/3}$

The theory of diffracted rays is invalid for points that are very close to the scattering obstacle, or too close to the shadow boundary. The special nature of the vicinity of the shadow boundary is apparent from Fig.2, from which it is seen that small values of $\theta_1 - \theta_o$ imply the close proximity of the points Q_o and Q_1, while the assumption regarding the independent nature of the diffraction processes at these points requires that they be not too close. We are therefore forced to seek an alternative representation for the solution in this shadow transition region, defined by $\theta_1 - \theta_o \lesssim (ka)^{-1/3}$, across which the character of the solution changes from that appropriate to the deep shadow to that for the illuminated region.

There are several lines of attack to deal with this transition zone, notably those due to Fock[4] and to Ludwig[5]. Fock writes the governing equations in a suitable system of 'ray coordinates' and simplifies the complicated equations that ensue for the short wave limit $ka \gg 1$; this is essentially a boundary layer approach in which a differential operator that corresponds to relatively slow longitudinal changes in amplitude is neglected in comparison

THIS DOCUMENT PROVIDED BY THE ABBOTT AEROSPACE
TECHNICAL LIBRARY
ABBOTTAEROSPACE.COM

with terms that represent the rapid transition across the shadow boundary. The approach adopted by Ludwig[5] is that of finding exact solutions, for sphere or circular cylinder, and expressing the short wave limit of these solutions in a form such that a generalisation for bodies of more general shape is suggested. Although this latter approach seems more powerful, in that it gives results even near the point of glancing incidence, where shadow boundary and surface intersect, Fock's analysis is simpler in concept and is favoured here.

Details are omitted, for the sake of brevity, but the main result of relevance in the present context is that the behaviour of the field across the transition region is determined in terms of a Fresnel integral (3-3) together with a 'Fock-function' g that is expressed in terms of Airy functions. In the notation of Fig.2, with incident field given again by

$$p_i = \left(\frac{\pi k}{2}\right)^{1/2} e^{i\pi/4} H_o^{(1)}(kR) \quad , \qquad R = |\underline{x}_1 - \underline{x}_o| \quad , \tag{5-1}$$

it is found that

$$p \sim M^{-1} (2\pi k)^{1/2} e^{i\pi/4} e^{ik(t_o+t_1+s)} \Phi\left(\frac{M}{a}(t_1+t_o+s); \frac{M^2 t_1^2}{a^2}, \frac{M^2 t_o^2}{a^2}\right) \quad , \tag{5-2}$$

in which the parameter $M = (\frac{1}{2}ka)^{1/3}$ is large, and Φ can be expressed as an integral involving Airy functions.

At large values of M, and for points not too close to the obstacle, ensured by taking Mt_o and Mt_1 also large, Fock[4] shows that the function Φ can be written in terms of a Fresnel integral that accounts for the essential structure of the pressure field across the shadow, together with an additional, relatively slowly varying, term that contributes a background sound field. Specifically, we have

$$\Phi(x;y_1,y_o) = \phi(x;y_1,y_o) + \psi(x;y_1,y_o) \quad , \tag{5-3}$$

where ϕ and ψ are estimated as follows. For large y_1 and y_o, with $\zeta = x - y_o^{1/2} - y_1^{1/2}$ finite or small, it is shown that

$$\phi(x;y_1,y_o) \sim (y_o y_1)^{-1/4} \frac{e^{-i\pi/2}}{2\pi} \mu F(\mu\zeta) \quad , \qquad \zeta > 0 \quad , \tag{5-4}$$

THIS DOCUMENT PROVIDED BY THE ABBOTT AEROSPACE
TECHNICAL LIBRARY
ABBOTTAEROSPACE.COM

wherein

$$\mu^2 = \frac{(y_o\, y_1)^{1/2}}{y_o^{1/2} + y_1^{1/2}} \quad \text{and} \quad \zeta = x - y_o^{1/2} - y_1^{1/2} = \frac{M}{a}\, s \quad . \qquad (5\text{-}5)$$

It is seen that $\zeta = (\tfrac{1}{2}ka)^{1/3}\, s/a$, whence $\zeta > 0$ corresponds to the shadow region, $\zeta = 0$ is the shadow boundary and $\zeta \lesssim 1$ corresponds to the transition region of present interest. Since $y_o^{1/2} = Mt_o/a = (\tfrac{1}{2}ka)^{1/3}\, t_o/a$ and $y_1^{1/2} = (\tfrac{1}{2}ka)^{1/3}\, t_1/a$, the requirement that y_o and y_1 be large corresponds to the condition that source and observer be not too close to the body.

As for the remaining function ψ of (5-3), this is expressed for large values of y_o and y_1 in the form

$$\psi(x;y_1,y_o) \sim -(y_o\, y_1)^{-1/4}\, \frac{1}{4\pi i}\, g(\zeta) \qquad (5\text{-}6)$$

where the 'Fock-function' $g(\zeta)$ is defined as

$$g(\zeta) = -\int_o^\infty \exp\left(-\zeta t\, e^{i\pi/6}\right) \frac{Ai'(t)}{Ai'(t\, e^{-\frac{2}{3}\pi i})}\, dt +$$

$$+ e^{-i\pi/3} \int_o^\infty e^{i\zeta t}\, \frac{Ai'(t)}{Ai'(t\, e^{-\frac{4}{3}\pi i})}\, dt \quad , \qquad (5\text{-}7)$$

a few properties of g being described in the appendix.

Adding together the estimates (5-4) and (5-6), we have, with reference to (5-2) and (5-3), the result that

$$p \sim \frac{a}{M^2}\left(\frac{k}{2\pi}\right)^{1/2} \frac{e^{-i\pi/4}\, e^{ik(t_1+t_o+s)}}{(t_1\, t_o)^{1/2}} \{\mu F(\mu\zeta) - \tfrac{1}{2}\, g(\zeta)\} \qquad (5\text{-}8)$$

in the transition region, with

$$\mu^2 = \frac{M}{a}\frac{t_o\, t_1}{t_o + t_1} \quad \text{and} \quad \zeta = \frac{M}{a}\, s \quad . \qquad (5\text{-}9)$$

Formula (5-8) gives the approximate pressure field at P_1 due to a source at P_o, and the far field limit $|\underline{x}_o| \to \infty$ is obtained by taking $t_o \to \infty$, whence

THIS DOCUMENT PROVIDED BY THE ABBOTT AEROSPACE
TECHNICAL LIBRARY
ABBOTTAEROSPACE.COM

$$\mu^2 \to \mu_1^2 = \frac{M}{a} t_1 \quad , \tag{5-10}$$

and

$$p \sim \frac{a}{M^2} \left(\frac{k}{2\pi}\right)^{1/2} \frac{e^{-i\pi/4} e^{ik(t_1+t_o+s)}}{(t_o t_1)^{1/2}} \{\mu_1 F(\mu_1 \zeta) - g(\zeta)\} \quad , \tag{5-11}$$

for $(ka)^{1/3} t_1 \gg 1$, $(ka)^{1/3} s \lesssim 1$.

It will be seen that the term in F corresponds to a Fresnel pattern very similar to that for a sharp edge, while the term in g provides a slowly varying background level. More precisely, within an 'inner transition region' given by $s = a(\theta_1 - \theta_o) \lesssim (ka)^{-1/2}$ the Fresnel term dominates the solution; towards the outer extremes of the transition region, where $s \approx (ka)^{-1/3}$, it is found that the two terms cancel to this order of approximation, this reflecting the fact that the solution for a rounded plate becomes <u>exponentially small</u> in the deep shadow. Within the 'outer transition region', $(ka)^{-1/3} \gtrsim s \gtrsim (ka)^{-1/2}$, the nature of the solution changes from the exponential behaviour appropriate to a convex obstacle to the Fresnel pattern like that of a sharp body.

(i) <u>Inner transition region</u>: $(ka)^{1/2} (\theta_1 - \theta_o) = O(1)$

If s is sufficiently small so that $(ka)^{1/2} s/a = O(1)$, then it is clear from (5-9) that

$$\zeta = \frac{M}{a} s = \frac{(\frac{1}{2}ka)^{1/3}}{a} s = O(ka)^{-1/6}$$

and is uniformly small. Thus $g(\zeta)$ may be replaced by its approximate value $g(0)$ and is negligible compared with the Fresnel term of (5-11), whence

$$p \sim \pi^{-1/2} e^{-i\pi/4} \frac{e^{ik(t_o+t_1+s)}}{t_o^{1/2}} F((\tfrac{1}{2}kt_1)^{1/2} (\theta - \theta_o)) \quad ,$$

and

$$\frac{p}{p_i} \sim \pi^{-1/2} e^{-i\pi/4} e^{iks} F((\tfrac{1}{2}kt_1)^{1/2} (\theta - \theta_o)) \quad . \tag{5-12}$$

A comparison of (5-12) with the corresponding result (3-6) for the half-plane shows that the two expressions are almost identical, differing only by a phase factor.

THIS DOCUMENT PROVIDED BY THE ABBOTT AEROSPACE
TECHNICAL LIBRARY
ABBOTTAEROSPACE.COM

(ii) Outer edge of transition region: $(ka)^{1/3}\ (\theta_1 - \theta_o) \gg 1$

As the observation point travels further toward the deep shadow, we know from section 4 that the solution becomes exponentially small, and we expect that the algebraic behaviour of F will therefore be cancelled by the background noise term g of formula (5-11). It is now verified that the leading terms do indeed cancel, making use of the fact that if $(ka)^{1/3}\ (\theta_1 - \theta_o)$ is large then the variables $\mu_1\zeta$ and ζ are both large, whence the functions $F(\mu_1\zeta)$ and $g(\zeta)$ of (5-11) may be replaced by their asymptotic forms given in the appendix. Thus we have

$$\mu_1 F(\mu_1\zeta) - \tfrac{1}{2}g(\zeta) \sim \mu_1 \frac{i}{2\mu_1\zeta} - \frac{1}{2\zeta} = 0 \quad ,$$

and the two terms cancel to this order, as indeed they must.

(iii) Outer transition region: $(ka)^{-1/3} \gtrsim (\theta_1 - \theta_o) \gtrsim (ka)^{-1/2}$

In this region the variable ζ changes from $\zeta = O(1)$, near the outer extreme $\theta_1 - \theta_o \approx (ka)^{-1/3}$, to $\zeta = O(ka)^{-1/6}$ when $\theta - \theta_o \approx (ka)^{-1/2}$. Thus the function g of (5-11) is a relatively slowly varying function that differs little from $g(0)$, and has only a background role in the pressure distribution; the role of $g(\zeta)$ is that of smoothing the pressure p from its exponentially small value in the deep shadow to the Fresnel pattern in the inner zone.

(iv) Shift of the shadow boundary

A secondary effect due to the background field term g is that of producing a slight shift in the geometrical shadow boundary, this effect being discussed by, among others, Keller[6] and Nussenzveig[7]. Apart from being of some interest in its own right, a calculation of this shift can be used in order to compare with earlier results, and provides a check of the validity of Fock's approximation used here for the transition region.

The geometrical optics limit $(ka = \infty)$ *predicts that* $p/p_i = \frac{1}{2}$ on the geometrical shadow boundary $\theta_1 = \theta_o$; if ka is finite, but large, then it is reasonable to define the shadow boundary by means of the definition

$$|p/p_i| = \tfrac{1}{2} \qquad (5\text{-}13)$$

and it remains to calculate the (small) value of $\theta_1 - \theta_o$ defined by (5-13). At points very close to the shadow boundary, where $s = a(\theta_1 - \theta_o)$ is small,

THIS DOCUMENT PROVIDED BY THE ABBOTT AEROSPACE
TECHNICAL LIBRARY
ABBOTTAEROSPACE.COM

the function $F(\mu_1\zeta)$ and $g(\zeta)$ of (5-11) may be replaced by their values for small argument, given in the appendix; thus

$$\mu_1 F(\mu_1\zeta) \sim \mu_1 \left(e^{i\pi/4} \frac{\sqrt{\pi}}{2} - \mu_1\zeta + \ldots \right)$$

and $g(\zeta) \sim g(0) \equiv 2^{1/3} C$, whence

$$\frac{p}{p_i} \sim \frac{1}{2} \left\{ 1 - \frac{2}{\sqrt{\pi}} e^{-i\pi/4} (\tfrac{1}{2}kt_1)^{1/2} \left[(\theta_1 - \theta_o) + \frac{a\,C}{(ka)^{2/3}\, t_1} \right] \right\} .$$

The definition (5-13) for the shadow boundary requires that

$$\Re\, e^{-i\pi/4} \left[(\theta_1 - \theta_o) + \frac{a\,C}{(ka)^{2/3}\, t_1} \right] = 0 ,$$

i.e.

$$(\theta_1 - \theta_o) = -\frac{a}{(ka)^{2/3}\, t_1} (\Re\, C + \Im\, C) = \frac{1.1806a}{(ka)^{2/3}\, t_1} \qquad (5\text{-}13)$$

This corresponds to a parallel displacement of the shadow boundary by a distance

$$d = 1.1806\, a\, (ka)^{-2/3} \qquad (5\text{-}14)$$

towards the shadow side. A similar calculation for the half-plane reveals a displacement proportional to wavelength $2\pi/k$, as indeed must be the case since this is the only length scale of the problem. It is found from (3-2) that the displacement is again towards the shadow side, and of magnitude

$$d_1 = 1/(k \sin \theta_o) , \qquad (5\text{-}15)$$

this being valid provided θ_o is not too small, namely for $(kr_1)^{1/2}\, \theta_o \gg 1$.

6 GENERALISATIONS

The work of sections 4 and 5, concerning the diffraction of sound by a convex obstacle, has dealt with the case of a perfectly rigid body whose curvature is constant along its curved part.

It is perhaps worthwhile to point out that the ideas involved can readily be extended to deal with the more general impedance condition

THIS DOCUMENT PROVIDED BY THE ABBOTT AEROSPACE
TECHNICAL LIBRARY
ABBOTTAEROSPACE.COM

$$\partial p/\partial n = i q p \quad , \quad q = \text{constant} \qquad (6\text{-}1)$$

and to allow for continuously changing curvature.

In the deep shadow for example, the basic structure of the solution (4-7) still holds. Variable curvature is accounted for by taking for the parameters b and α their local values $b(Q(\rho))$ and $\alpha(\rho(s))$, where ρ denotes the local radius of curvature at s. The solution for an imperfectly rigid boundary, with condition (6-1), simply requires this boundary condition to be employed in the exact solution for circular cylinder that is used to extract values for the local diffraction coefficients b and α. A general treatment of such problems can be found in the work of Keller and Levy[2], which deals with both two- and threedimensional bodies.

Turning now to the shadow transition region, the solution (5-2) in terms of ray coordinates t_o, t_1 and s holds even for bodies of variable curvature. As for a more general boundary condition, such as (6-1), Fock shows that the character of the solution remains unchanged: it is found that the value of the impedance q affects only the Fock function, g, of formulae (5-8) and (5-11), and leaves the Fresnel integral term unchanged. That is to say, the Fresnel diffraction pattern remains unchanged, while the value of the impedance affects only the slowly varying background sound field.

Finally, it is remarked that although the results so far have been restricted to the case in which source and observation points lie in the same plane normal to the generators of the scatterer, this restriction can be removed by a simple analysis, as is now shown.

If the incident field is that of source given by

$$p_i = e^{ikR}/R \quad , \qquad R = |\underline{x}_o - \underline{x}_1| \quad ,$$

the far field limit is obtained by taking $|\underline{x}_o| \to \infty$, now in any direction. Thus

$$R \sim r_o + \underline{\alpha} \cdot \underline{x}_1 \quad , \qquad (6\text{-}2)$$

where $\underline{\alpha} = -\underline{x}_o/r_o$ is the unit vector from $\underline{x}_o$ towards an origin near $\underline{x}_1$. If $\underline{\alpha}$ has direction cosines

THIS DOCUMENT PROVIDED BY THE ABBOTT AEROSPACE
TECHNICAL LIBRARY
ABBOTTAEROSPACE.COM

$$\underline{\alpha} = (\cos\theta_o \cos\lambda_o , \sin\theta_o \cos\lambda_o , \sin\lambda_o) \quad , \tag{6-3}$$

then the work considered hitherto is recovered by setting $\lambda_o = 0$. With general values of λ_o, on the other hand, the incident field takes the plane wave form

$$p_i \sim \frac{e^{ikr_o}}{r_o} \exp\{ik (x_1 \cos\theta_o \cos\lambda_o + y_1 \sin\theta_o \cos\lambda_o + z_1 \sin\lambda_o)\} , \tag{6-4}$$

i.e.

$$p_i \sim A_1 e^{ik\cos\lambda_o (x_1\cos\theta_o + y_1\sin\theta_o)} , \tag{6-5}$$

where $A_1 = (e^{ikr_o}/r_o)\, e^{ikz_1\sin\lambda_o}$, and $k \cos\lambda_o$ is the wave number component in the plane perpendicular to the generators of the scatterer.

It is seen that the multiplicative factor A_1 will appear throughout the problem, having only the effect of replacing the wave equation (1-2) by

$$(\nabla^2 + k^2 \cos^2\lambda_o)\, p = 0 \quad . \tag{6-6}$$

Now the governing equations (6-6), with (6-5) as incident field, together with the rigid boundary condition $\partial p/\partial n$, are seen to be exactly the same as in the case of normal incidence previously considered, with the wave number k reduced to $k \cos\lambda_o$. It follows that all our results, for the ratio p/p_i of total against incident pressure, can be modified to include oblique incidence by changing k to $k \cos\lambda_o$ throughout.

7 CONCLUSIONS

A comparison has been made between the distant pressure fields in shadows cast by sharp and smooth ended obstacles, and the main results are summarised here for reference.

A source is situated at $P_1(\underline{x}_1)$, and an observer $P_o(\underline{x}_o)$ at great distance from the body measures the induced pressure field. Within the deep shadow region, where $(\theta_1 - \theta_o)(ka)^{1/3} \gg 1$, the field cast by a smooth sided body is much less than that due to a half-plane.

Thus

$$|p/p_i|_{\text{half-plane}} \sim \tfrac{1}{2}\pi^{-1/2} (2kt_1)^{-1/2} \{\operatorname{cosec} \tfrac{1}{2}(\theta_1 - \theta_o) + \operatorname{cosec} \tfrac{1}{2}(\theta_1 + \theta_o)\} \quad \ldots. \tag{7-1}$$

THIS DOCUMENT PROVIDED BY THE ABBOTT AEROSPACE TECHNICAL LIBRARY ABBOTTAEROSPACE.COM

and

$$|p/p_i|_{smooth} \sim 1.08\ (ka)^{1/3}\ (kt_1)^{-1/2}\ \exp\ (-\ 0.700\ (ka)^{1/3}(\theta_1 - \theta_o))\ . \quad (7\text{-}2)$$

It is seen that the former solution exhibits algebraically small decay, while the latter has exponential decay, in the short wave limit $ka \gg 1$.

Within the shadow transition region, $(ka)^{1/3}\ (\theta_1 - \theta_o) \lesssim 1$, the two solutions have similar behaviour; given by (3-6) and (5-11). The solution (5-11) for the rounded body consists of two terms that correspond to a Fresnel diffraction like that for the half-plane, together with a relatively slowly varying background field g.

In the inner transition region, $(ka)^{1/2}\ (\theta_1 - \theta_o) \lesssim 1$, the background term is negligible, whence it is found that the solutions for half-plane and rounded body are asymptotically identical, apart from a phase change. Specifically, we have

$$|p/p_i| \sim \pi^{-1/2}\ |F((\tfrac{1}{2}kt_1)^{1/2}\ (\theta_1 - \theta_o))| \quad (7\text{-}3)$$

for either sharp or rounded ends.

Within the remaining outer transition zone, $(ka)^{-1/2} \lesssim \theta_1 - \theta_o \lesssim (ka)^{-1/3}$, the background function g of (5-11) has the role of smoothing the pressure distribution from its exponentially small deep shadow behaviour to that of the Fresnel pattern near the shadow.

These results are appropriate to the short wave asymptotic limit $ka \to \infty$, and it is important to estimate how large ka must be for their validity to be ensured. It is seen from (7-2) that the decay in the deep shadow requires that $(ka)^{1/3}$ be large, and consequently that ka must be very large. If formula (7-2) is to be valid for angles $\theta_1 - \theta_o \geqslant 10^o$ (i.e. 1/6 radian), then the requirement of small exponential term implies that

$$0.12\ (ka)^{1/3} \gg 1\ ,$$

i.e.

$$ka \gg 600\ ; \quad (7\text{-}4)$$

evidently the nondimensional wave number ka should be of order 1000 or more, to ensure the validity of (7-2) as a sensible approximation.

THIS DOCUMENT PROVIDED BY THE ABBOTT AEROSPACE
TECHNICAL LIBRARY
ABBOTTAEROSPACE.COM

Finally, for the case of sound waves, the intensity within the shadow for both sharp and rounded bodies is calculated, using (7-1), (7-2) and (7-3) and plotted in Fig.5. The radius a is taken as 1.3 metres, $r_1 = t_1 = 10$ metres, with frequencies 1 kHz, 10 kHz, 100 kHz, corresponding to values of ka of 25, 250, 2500 respectively. The function $I = 20 \log_{10} |p/p_i|$ gives the sound intensity in decibels (dB), and this is plotted against $\theta_1 - \theta_o$, the angular position of the observer with respect to the shadow boundary.

In Part B, the case of variable radius of curvature $\rho(\theta)$ is examined, with a view to choosing a shape such that the exponential decay in the shadow is as great as possible.

This Document Provided by the Abbott Aerospace
Technical Library
abbottaerospace.com

THIS DOCUMENT PROVIDED BY THE ABBOTT AEROSPACE
TECHNICAL LIBRARY
ABBOTTAEROSPACE.COM

Appendix

SPECIAL FUNCTIONS

A.1 Fresnel function

The Fresnel integral $F(x)$ is defined as

$$F(x) = e^{-ix^2} \int_x^\infty e^{it^2}\, dt \quad . \tag{A-1}$$

Setting $x = 0$, we have

$$F(0) = \int_0^\infty e^{it^2}\, dt \quad ,$$

and this can be evaluated by deforming the path of integration from the origin to $\infty e^{i\pi/4}$, whence

$$F(0) = e^{i\pi/4} \int_0^\infty e^{-s^2}\, ds = \tfrac{1}{2}\pi^{1/2}\, e^{i\pi/4} \quad .$$

To find the value of $F(x)$ for small x, we may use this result by writing

$$e^{ix^2} F(x) = F(0) - \int_0^x e^{it^2}\, dt \quad , \tag{A-2}$$

and the latter integral may be expanded and integrated term-by-term, to get

$$F(x) = \tfrac{1}{2}\pi^{1/2}\, e^{i\pi/4} - x + \ldots \quad . \tag{A-3}$$

To estimate F for large positive x, substitute $s = (t/x)^2 - 1$, then rotate the path of integration through $\pi/2$ to get

$$F(x) = \frac{ix}{2} \int_0^\infty e^{-x^2 t}\, (1 + it)^{-1/2}\, dt \quad , \qquad x > 0 \ .$$

For large values of x^2, the main contribution arises from the vicinity of $t = 0$, whence the asymptotic expansion is obtained, according to Watson's lemma, by formally expanding $(1 + it)^{-1/2}$ and integrating term-by-term. Thus

$$F(x) \sim \frac{i}{2x} + \ldots \qquad \text{as} \quad x \to +\infty \quad . \tag{A-4}$$

THIS DOCUMENT PROVIDED BY THE ABBOTT AEROSPACE TECHNICAL LIBRARY ABBOTTAEROSPACE.COM

For large and negative values of x, an estimate is obtained by use of the fact that the integral on the right side of (A-2) is an odd function of x, whence

$$e^{ix^2} F(x) - F(0) = - e^{ix^2} F(-x) + F(0)$$

which may be expanded as $x \to -\infty$, using (A4), to get

$$F(x) \sim \pi^{1/2} e^{i\pi/4} e^{-ix^2} + \frac{i}{2x} + \ldots \quad . \tag{A-5}$$

A.2 Airy function

The Airy function $Ai(z)$ satisfies the equation

$$Ai''(z) = z\, Ai(z) \quad , \tag{A-6}$$

together with the boundary condition at infinity:

$$Ai \sim \tfrac{1}{2}\pi^{-1/2} z^{-1/4} \exp\left(-\frac{2}{3} z^{3/2}\right) \quad , \quad |z| \to \infty, |\arg z| < \pi \ . \tag{A-7}$$

A second independent solution Bi of equation (A-6) is specified by the requirement:

$$Bi \sim \pi^{-1/2} z^{-1/4} \exp\left(+\frac{2}{3} z^{3/2}\right) \quad , \quad |z| \to \infty \ |\arg z| < \pi/3 \quad .$$

The zeros of Ai and Ai' are real and negative. In particular, if $-a_o$, $-a_1$, $-a_2$, ... denote the zeros of $Ai'(z)$, numbered in ascending magnitude, then

$$a_o = 1.0188... \quad , \quad a_1 = 3.2482... \quad , \tag{A-8}$$

with

$$Ai(a_o) = 0.5357... \ , \ Ai(a_1) = -0.4190... \quad . \tag{A-9}$$

There are several different notations in common use for the Airy functions. That used by Keller[2], for example, is the function $A(z)$ related to Ai by the identity

THIS DOCUMENT PROVIDED BY THE ABBOTT AEROSPACE
TECHNICAL LIBRARY
ABBOTTAEROSPACE.COM

$$A(z) = 3^{-1/3}\,\pi\,Ai(-3^{-1/3}z) \quad ,$$

whence the zeros q_n of $A(z)$ are given by $q_n = 3^{1/2}\,a_n$.

A.3 Fock function

The Fock function $g(\zeta)$ is defined in terms of the Airy function Ai by the integral

$$g(\zeta) = -\int_0^\infty e^{-\zeta t e^{i\pi/6}} \frac{Ai'(t)}{Ai'(t\,e^{-\frac{2}{3}\pi i})}\,dt + e^{-i\pi/3}\int_0^\infty e^{i\zeta t}\frac{Ai'(t)}{Ai'(t\,e^{-\frac{4}{3}\pi i})}\,dt \quad . \qquad \ldots\ (A\text{-}10)$$

When ζ is large and positive, the main contribution to the integrals arises from the vicinity of $t = 0$, and since Ai' is analytic near this point, we have

$$g(\zeta) \sim -\frac{1}{\zeta\,e^{i\pi/6}} - \frac{e^{-i\pi/3}}{i\zeta}$$

i.e.

$$g(\zeta) \sim i/\zeta \qquad \text{as} \quad \zeta \to +\infty \ . \qquad (A\text{-}11)$$

When $\zeta = 0$, we have

$$g(0) = -\int_0^\infty \frac{Ai'(t)}{Ai'(t\,e^{-\frac{2}{3}\pi i})}\,dt + e^{-i\pi/3}\int_0^\infty \frac{Ai'(t)}{Ai'(t\,e^{-\frac{4}{3}\pi i})}\,dt \quad .$$

Apart from a constant factor, this is the same constant C as that discussed by Keller and Rubinov[6], in a slightly different notation. Thus

$$g(0) = 2^{1/3}\,C \quad , \qquad (A\text{-}12)$$

and the constant C is given[6] to several decimal places, whence

$$g(0) = 0.4321\,2^{4/3}\,e^{i\pi/3} \qquad (A\text{-}13)$$

THIS DOCUMENT PROVIDED BY THE ABBOTT AEROSPACE
TECHNICAL LIBRARY
ABBOTTAEROSPACE.COM

REFERENCES

No.	Author(s)	Title, etc.
1	J.B Keller	Diffraction by a convex cylinder. IRE Trans. Ant. Propag., AP4, 312 (1956)
2	J.B. Keller B.R. Levy	Diffraction by a smooth object. Comm. Pure Appl. Math., 12, 159 (1959)
3	H.M. MacDonald	A class of diffraction problems. Proc. Lond. Math. Soc. (2), 14, 410 (1915)
4	V.A. Fock	Electromagnetic diffraction and propagation problems. Pergamon (1965)
5	D. Ludwig	Uniform asymptotic expansion of the field scattered by a convex object at high frequencies. Comm. Pure Appl. Math., 20, 103 (1967)
6	J.B. Keller S.I. Rubinow	Shift of the shadow boundary and scattering cross section of an opaque object. J. Appl. Phys. 32, 814 (1961)
7	H.M. Nussenzveig	High frequency scattering by an impenetrable sphere. Ann. Phys. 34, 23 (1965)

THIS DOCUMENT PROVIDED BY THE ABBOTT AEROSPACE
TECHNICAL LIBRARY
ABBOTTAEROSPACE.COM

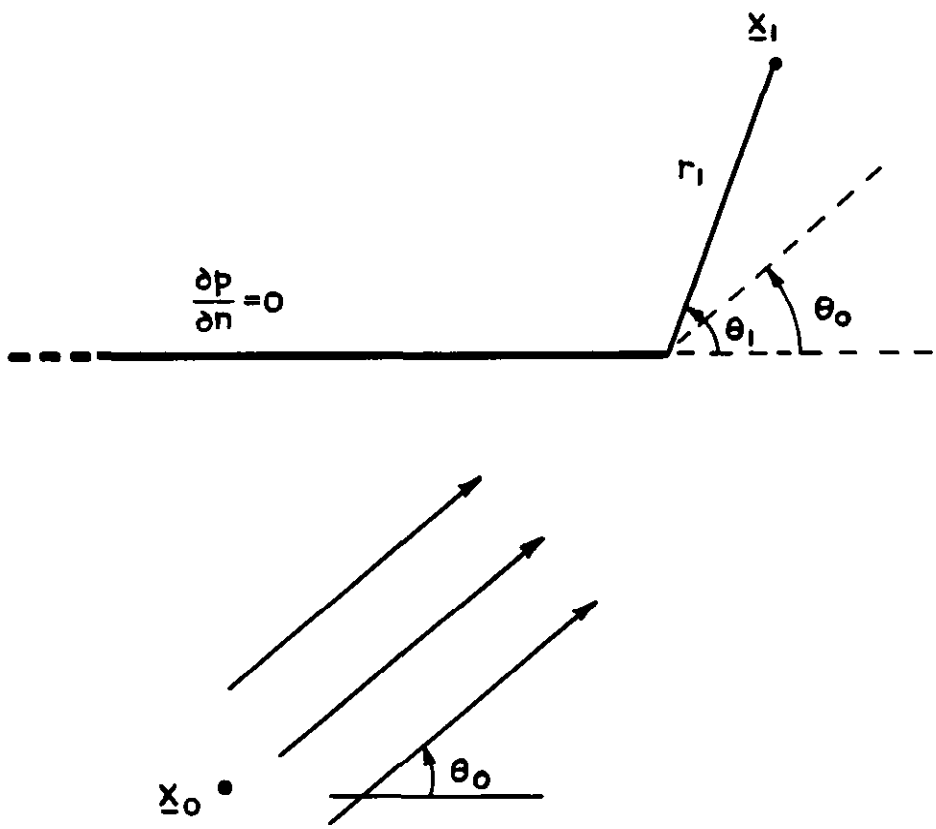

θ_0 denotes the angle of incidence, with $0 < \theta_0 < \pi$: the shadow region is defined by $\theta_0 < \theta_1 < \pi$. The direction of the wave is $\underline{\alpha} = (\cos\theta_0, \sin\theta_0)$ and $\underline{x}_0 = -\underline{\alpha}\,|\underline{x}_0|$ is a point at great distance from the edge

Fig.1 Geometry for the rigid half plane

THIS DOCUMENT PROVIDED BY THE ABBOTT AEROSPACE
TECHNICAL LIBRARY
ABBOTTAEROSPACE.COM

$P_o Q_o$ and $Q_1 P_1$ are tangents to the surface, and are at angles θ_o and θ_1 to the positive x- direction. The deep shadow is the region $\theta_1 - \theta_o \gg (ka)^{-1/3}$, and at distance $\gg a\,(ka)^{-1/3}$ from the body

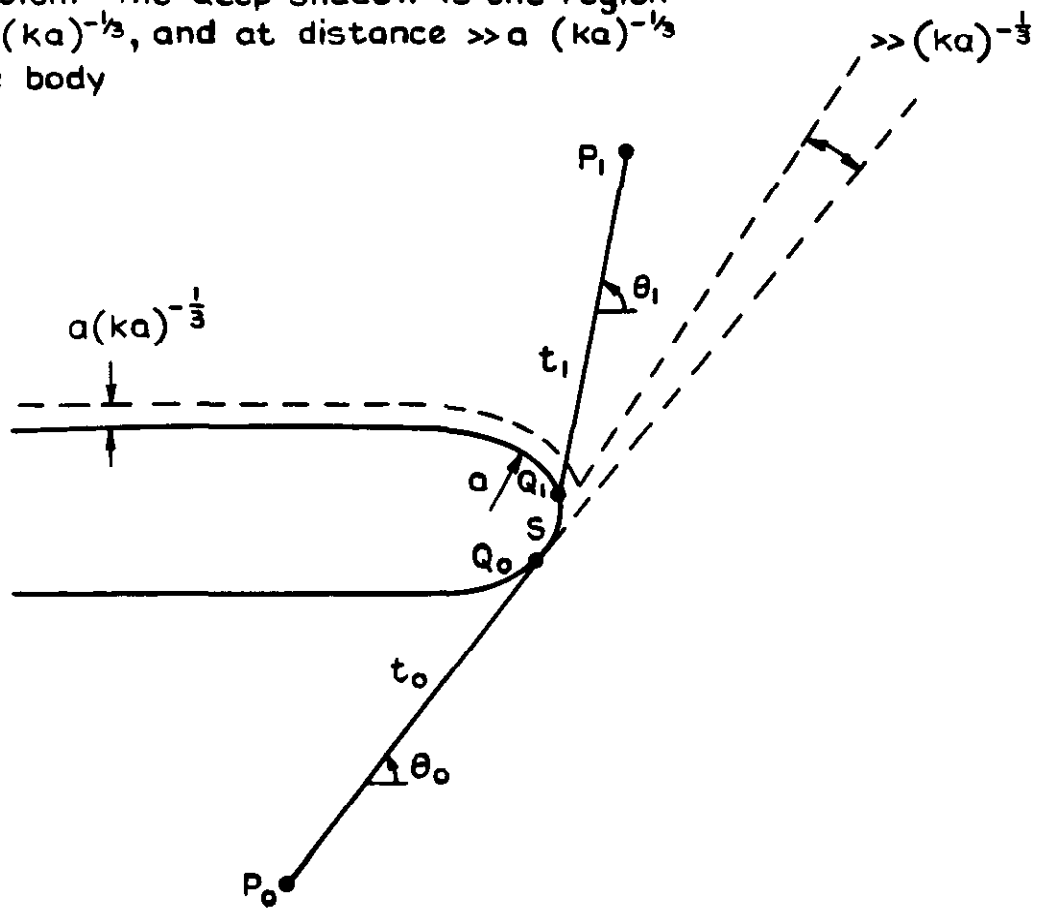

Fig.2 Geometry for a rounded body

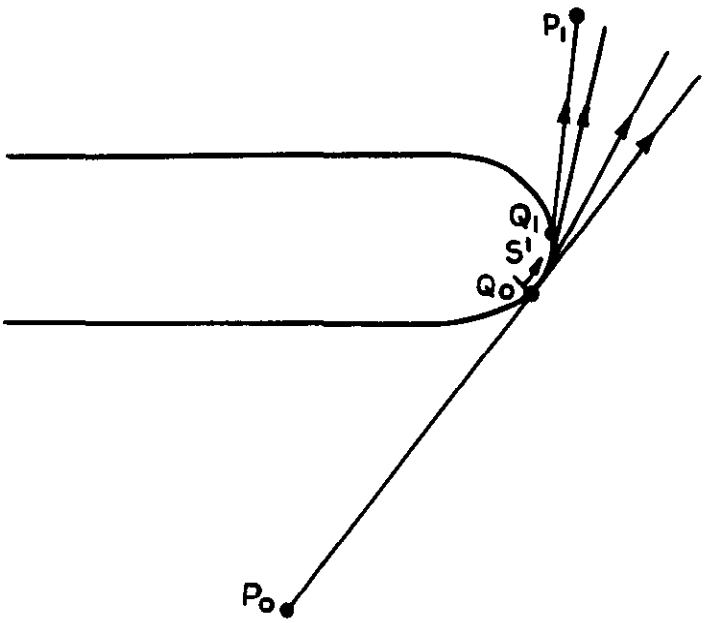

Fig.3 Diffracted rays are shed in tangential directions: the envelope of these rays is the curved section of the body

THIS DOCUMENT PROVIDED BY THE ABBOTT AEROSPACE
TECHNICAL LIBRARY
ABBOTTAEROSPACE.COM

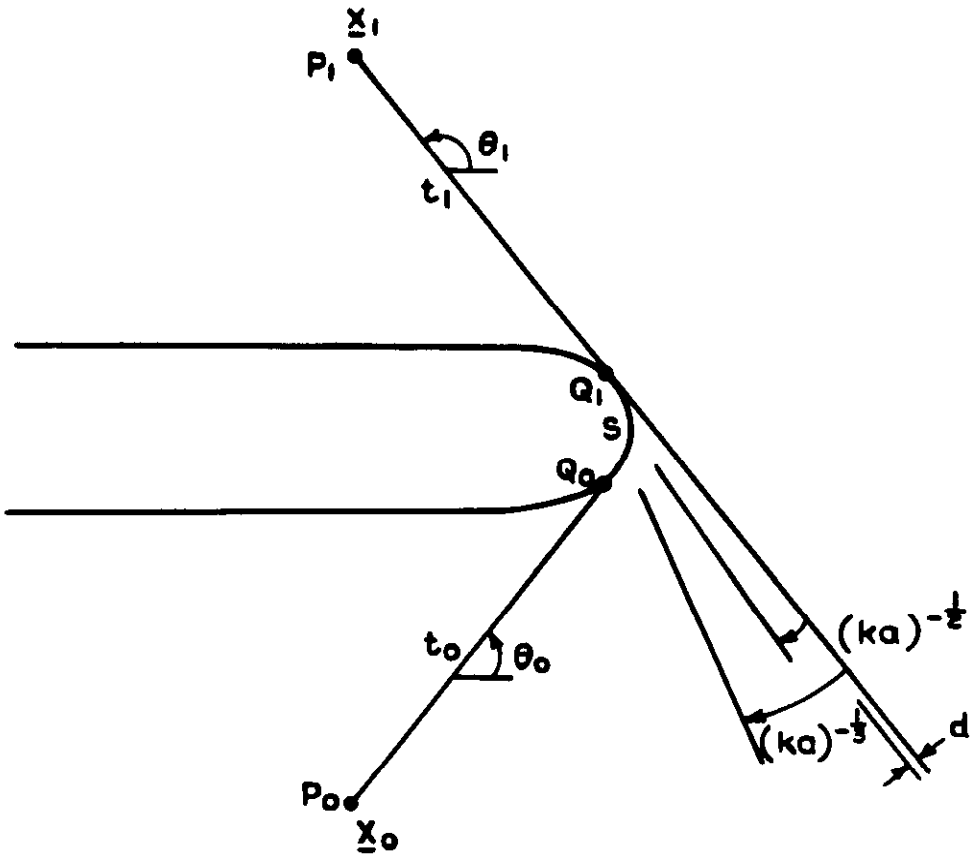

$P_1Q_1 = t_1$, $P_0Q_0 = t_0$, $Q_1Q_0 = S$. The deep shadow is given by $\theta_1 - \theta_0 >> (ka)^{-\frac{1}{3}}$, the shadow transition region is given by $\theta_1 - \theta_0 \lesssim (ka)^{-\frac{1}{3}}$ and the inner transition region is given by $\theta_1 - \theta_0 \lesssim (ka)^{-\frac{1}{2}}$. The geometrical shadow boundary is shifted by the displacement d

Fig.4 Shadow regions for rounded body

THIS DOCUMENT PROVIDED BY THE ABBOTT AEROSPACE
TECHNICAL LIBRARY
ABBOTTAEROSPACE.COM

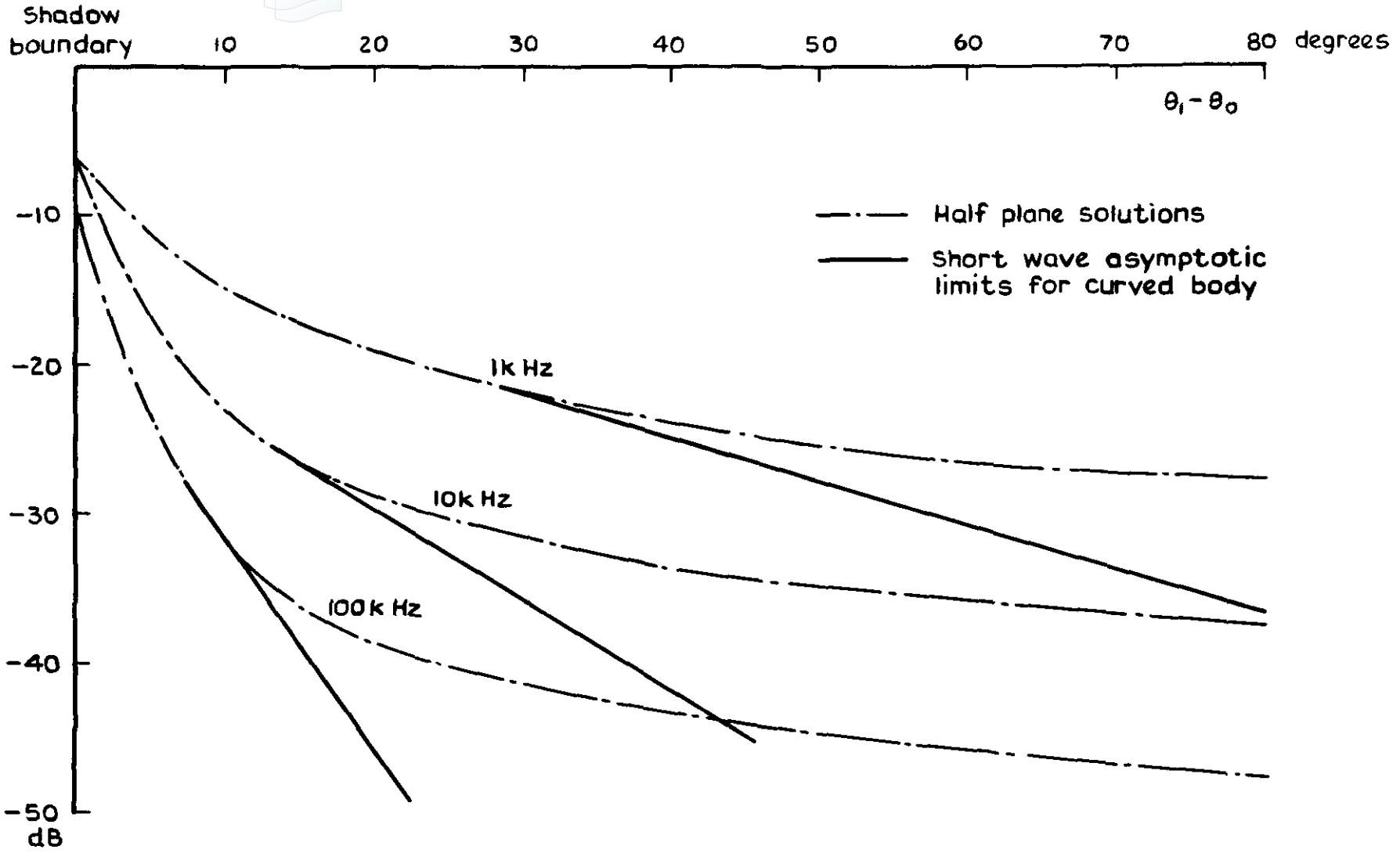

Fig.5 Intensity, $I = 20 \log_{10} |P/P_i|$ against angle into shadow, $\theta_1 - \theta_0$

THIS DOCUMENT PROVIDED BY THE ABBOTT AEROSPACE
TECHNICAL LIBRARY
ABBOTTAEROSPACE.COM

PART B

OPTIMISATION OF THE CURVATURE

1 INTRODUCTION

The idea of 'diffracted rays' that propagate energy into the shadow region cast by a convex body predicts a field that is exponentially small in the short wave limit $k\rho \to \infty$, where k is the radian wave number and ρ is a typical radius of curvature of the obstacle. Specifically, it has been shown in Part A, formulae ((4-7) - (4-9)), that the field within the 'deep shadow', not too close to the body or to the shadow boundary, has the asymptotic form

$$|p/p_i| \sim \frac{1.08\,[\rho(Q_o)\,\rho(Q_1)]^{1/6}}{k^{1/6}\,t_1^{1/2}} \exp\left(-0.70\,k^{1/3}\int_{\theta_o}^{\theta_1}\rho^{1/3}(\theta)\,d\theta\right), \qquad (1\text{-}1)$$

$$k\rho \gg 1, \quad (k\rho)^{1/3}(\theta_1 - \theta_o) \gg 1 \quad ,$$

where $\rho(\theta)$ denotes the local radius of curvature.

It is seen that the crucial exponential term of this expression has a decay rate that is proportional to the integral

$$I(\theta) = \int \rho^{1/3}(\theta)\,d\theta \quad , \qquad (1\text{-}2)$$

when the wave number k is fixed, and the value of I clearly depends upon details of the geometry of the scattering surface.

It is the object of this Report to examine how $I(\theta)$ can be made as large as possible by choosing suitable curves, subject to certain restraints imposed by the overall dimensions of the surface, in order that the shadow field be minimised.

2 BASIC MAXIMISATION PROCEDURE

Suppose Q_o and Q_1 are fixed points with coordinates (0,0) and (a,b) in the coordinate system of Fig.1, and a curve S has to be chosen so that S passes through Q_o and Q_1 at given angles θ_o and θ_1 to the horizontal. Our problem is to find the curve S such that the integral

$$I = \int_{\theta_o}^{\theta_1} \rho^{1/3}(\theta)\,d\theta \qquad (2\text{-}1)$$

is maximised, where ρ denotes the radius of curvature of S at an intermediate point $Q(\theta)$.

THIS DOCUMENT PROVIDED BY THE ABBOTT AEROSPACE
TECHNICAL LIBRARY
ABBOTTAEROSPACE.COM

It is therefore required that the functional (2-1) be maximised, subject to the constraints that Q_o and Q_1 lie on S, whence

$$a = \int_{\theta_o}^{\theta_1} \rho \cos\theta \, d\theta \quad \text{and} \quad b = \int_{\theta_o}^{\theta_1} \rho \sin\theta \, d\theta \, . \tag{2-2}$$

The required curve $\rho = \rho(\theta)$ is readily found by the standard procedure of variational calculus: introducing a pair of parameters, μ and λ, to be determined, we write

$$F(\rho,\theta) = \rho^{1/3} - \frac{1}{3}\mu\rho\cos\theta - \frac{1}{3}\lambda\rho\sin\theta \tag{2-3}$$

and have to maximise the integral

$$I_1 = \int_{\theta_o}^{\theta_1} F(\rho,\theta)\, d\theta \quad , \tag{2-4}$$

subject to the constraints (2-2). The governing Euler equation to determine F has the standard form

$$\frac{\partial F}{\partial \rho} = \frac{d}{d\theta}\left(\frac{\partial F}{\partial \rho'}\right) \tag{2-5}$$

and the right hand side of the equation is obviously zero in the present case, since $\rho' = d\rho/d\theta$ does not appear in the expression (2-3) for F. Thus the Euler equation (2-5) is a trivial one, with solution

$$\rho^{-2/3} = \mu\cos\theta + \lambda\sin\theta \quad , \tag{2-6}$$

and this defines the required curve. The parameters μ and λ are determined from the constraints (2-2), whence

$$a = \int_{\theta_o}^{\theta_1} \frac{\cos\theta\, d\theta}{(\mu\cos\theta + \lambda\sin\theta)^{3/2}} \quad \text{and} \quad b = \int_{\theta_o}^{\theta_1} \frac{\sin\theta\, d\theta}{(\mu\cos\theta + \lambda\sin\theta)^{3/2}} \, . \tag{2-7}$$

The pair of equations (2-7) is sufficient to calculate μ and λ, whence $\rho(\theta)$ is given by (2-6). In particular the maximum value of the integral (2-1) takes the value

THIS DOCUMENT PROVIDED BY THE ABBOTT AEROSPACE
TECHNICAL LIBRARY
ABBOTTAEROSPACE.COM

$$I_m = \int_{\theta_o}^{\theta_1} \frac{d\theta}{(\mu \cos\theta + \lambda \sin\theta)^{1/2}} = \int_{\theta_o}^{\theta_1} \frac{(\mu \cos\theta + \lambda \sin\theta)\, d\theta}{(\mu \cos\theta + \lambda \sin\theta)^{3/2}}$$

i.e.

$$I_m = \mu a + \lambda b \quad . \tag{2-8}$$

Although formulae (2-7) and (2-6) determine the curve $\rho(\theta)$ in principle for quite general values of a and b, the evaluation of μ and λ from the simultaneous integrals (2-7) is in general a formidable task. Our attention will henceforth be confined, therefore, to a particular limiting case, namely that of $b \ll a$. The angle θ_o will also be taken as zero for convenience, although the analysis can be carried out without this stipulation.

3 LIMIT $b/a \ll 1$ AND $\theta_1 \ll 1$

Here and henceforth the ratio b/a will be taken as small. It is found that the solution of (2-7) and (2-6) has a different form according as θ_1 is comparable with, or greater than, the small parameter $\varepsilon = b/a$, and our attention is directed firstly to the case in which θ_1 is also small. Thus $\varepsilon = b/a \ll 1$ and $\theta_1 \ll 1$, with no restrictions on their relative magnitudes.

For small θ_1, the trigonometrical functions in (2-7) may be uniformly approximated to get

$$a \approx \int_o^{\theta_1} \frac{d\theta}{(\mu + \lambda\theta)^{3/2}} = \frac{2}{\lambda}\{\mu^{-1/2} - (\mu + \lambda\theta)^{-1/2}\} \tag{3-1}$$

and

$$b \approx \int_o^{\theta_1} \frac{\theta\, d\theta}{(\mu + \lambda\theta)^{3/2}} = \frac{2}{\lambda^2}\{2(\mu + \lambda\theta_1)^{1/2} - 2\mu^{1/2} - \lambda\theta_1 (\mu + \lambda\theta_1)^{-1/2}\} \tag{3-2}$$

This pair of equations may be inverted to find μ and λ, thus

$$\lambda = (\theta_1 - 2\varepsilon)(2/b)^{2/3} (\theta_1 - \varepsilon)^{-2/3} \quad , \quad \mu = (2/b)^{2/3} \varepsilon^2 (\theta_1 - \varepsilon)^{-2/3} \tag{3-3}$$

where $\varepsilon = b/a$, and ρ is then given by

$$\rho(\theta) = (\mu \cos\theta + \lambda \sin\theta)^{-2/3} \approx (\mu + \lambda\theta)^{-2/3} \quad . \tag{3-4}$$

THIS DOCUMENT PROVIDED BY THE ABBOTT AEROSPACE
TECHNICAL LIBRARY
ABBOTTAEROSPACE.COM

According to formula (2-8), the maximum value of the integral (2-1) is

$$I_m = 2^{2/3}\, b^{1/3}\, (\theta_1 - b/a)^{1/3} \quad , \tag{3-5}$$

to this order of approximation. If we now allow the parameter b to vary, subject to the restriction $b < b_m$, we see that the maximum value of (3-5) occurs when b is chosen so that $(b/a) = \frac{1}{2}\theta_1$, provided $\frac{1}{2}\theta_1 \leqslant b_m/a$; otherwise the greatest value of (3-5) occurs when b assumes its largest value b_m. Thus

$$I_{max}(\theta_1) = \begin{cases} a^{1/3}\, \theta_1^{2/3} & \text{if } \theta_1 \leqslant 2b_m/a \\ 2^{2/3}\, b_m^{1/3}\, (\theta_1 - b_m/a)^{1/3} & \text{if } \theta_1 \geqslant 2b_m/a \quad . \end{cases} \tag{3-6}$$

A general picture of the function $I_{max}(\theta)$ appears in Fig.2, with a specific example in Fig.3.

It is important to note that for a given curve of the family (3-4), this maximum is attained only at the angle $\theta = \theta_1$, and it is of interest to calculate the value of the integral

$$I(\theta) = \int_0^{\theta} \rho^{1/3}(\theta')\, d\theta'$$

for values of θ other than $\theta = \theta_1$, with ρ given by (3-4), (3-3); it is seen that I is given by $I_{max}(\theta_1)$ when $\theta = \theta_1$, with $I(\theta) \leqslant I_{max}(\theta)$ for all other values of $\theta \neq \theta_1$.

To calculate the value of $I(\theta)$, formula (3-4) is substituted into the integral above and leads to the result that

$$I(\theta) = 2^{2/3}\, b^{1/3}\, \frac{(\theta_1 - \varepsilon)^{1/3}}{(\theta_1 - 2\varepsilon)} \{(\varepsilon^2 + \theta(\theta_1 - 2\varepsilon))^{1/2} - \varepsilon\} \quad , \tag{3-7}$$

for $\varepsilon = b/a \ll 1$ and $\theta_1 \ll 1$. In this formula, $b = \frac{1}{2}a\theta_1$ or $b = b_m$ according as $\theta_1 \leqslant 2b_m/a$ or $\theta_1 \geqslant 2b_m/a$. The apparent singularity in formula (3-7) at $\theta_1 = 2\varepsilon$, when the denominator becomes zero, is rendered negligible by the simultaneous vanishing of the numerator. In this case, the expression for I is obtained by letting $\varepsilon \to \frac{1}{2}\theta_1$, or else directly from (3-3), whence it is found that

THIS DOCUMENT PROVIDED BY THE ABBOTT AEROSPACE
TECHNICAL LIBRARY
ABBOTTAEROSPACE.COM

$$I(\theta) = (a/\theta_1)^{1/3}\,\theta \quad , \qquad b/a \ll 1,\ \theta_1 \lesssim 1,\ \theta < \theta_1 \quad .$$

This linear dependence on θ corresponds to the fact that the curve S, in this limit, has constant radius of curvature (a/θ_1): evidently this radius is large when θ_1 is small, and $I(\theta)$ quickly assumes a large value as θ increases to θ_1.

Graphs of $I(\theta)$, given by (3-7), appear in Fig.3, with $a = 6$ metres, $b_m = 1$ metre and with three different values of θ_1, namely
(a) $\theta_1 = \frac{1}{9}\ (\theta_1 < 2b_m/a)$, (b) $\theta_1 = \frac{1}{3}\ (\theta_1 = 2b_m/a)$ and (c) $\theta_1 = \frac{\pi}{2}$.

Although equation (3-4), together with (3-3), uniquely specifies the optimum curve, this functional form is not ideal for sketching its shape. A transformation to a more convenient parametric representation in terms of Cartesian coordinates $x(\theta)$ and $y(\theta)$ follows from the identities

$$x(\theta) = \int_0^\theta \rho(\theta')\cos\theta'\,d\theta' \quad \text{and} \quad y(\theta) = \int_0^\theta \rho(\theta')\sin\theta'\,d\theta' \quad ,$$

whence for the present case of small angles θ, we have

$$x(\theta) \approx \int_0^\theta \frac{d\theta'}{(\mu + \lambda\theta')^{3/2}} \quad \text{and} \quad y(\theta) \approx \int_0^\theta \frac{\theta'\,d\theta'}{(\mu + \lambda\theta')^{3/2}} \quad . \qquad (3\text{-}8)$$

The integrals of (3-8) can be evaluated explicitly, and the parameter θ may be eliminated to obtain an equation giving x in terms of y, thus

$$y = \varepsilon^2 x^2/\{a(\theta_1 - \varepsilon) - x(\theta_1 - 2\varepsilon)\} \quad , \qquad (3\text{-}9)$$

where $\varepsilon = b/a$ is small. Again, the value of b is $\frac{1}{2}a\theta_1$ or b_m, according as $\theta_1 \leqslant 2b_m/a$ or $\theta_1 \geqslant 2b_m/a$. Graphs are shown on Fig.4, with specific values assigned to a, b and θ_1.

4 LIMIT $b/a \ll 1$, $b/a \ll \theta_1$

Section 3 deals with the case where θ_1 is comparable with b/a, and the present analysis for $b/a \ll \theta_1$ provides information for the remaining range of values of θ_1.

It is seen from (3-3) that μ becomes small compared with λ when θ_1 increases to a value comparable with or greater than b/a; it is found in the present case $(\theta_1 \gg b/a)$ that this property must be maintained in order that

THIS DOCUMENT PROVIDED BY THE ABBOTT AEROSPACE
TECHNICAL LIBRARY
ABBOTTAEROSPACE.COM

the constants a and b given by (2-7) are such that $a \gg b$. Thus we have $\mu \ll \lambda$, and (2-7) simplifies to give

$$b \approx \int_0^{\theta_1} \frac{\sin\theta \, d\theta}{(\lambda \sin\theta)^{3/2}} \qquad (\text{if } \mu \ll \lambda\, \theta_1)$$

i.e.

$$b \approx \lambda^{-3/2} J(\theta_1) \tag{4-1}$$

where

$$J(\theta_1) = \int_0^{\theta_1} (\sin t)^{-1/2} \, dt \quad . \tag{4-2}$$

Similarly,

$$a = \int_0^{\theta_1} \frac{\cos\theta \, d\theta}{(\mu \cos\theta + \lambda \sin\theta)^{3/2}} = -\frac{2}{\lambda}\{(\mu + \lambda \sin\theta_1)^{-1/2} - \mu^{-1/2}\}$$

i.e.

$$a \approx 2/(\lambda\mu^{1/2}) \qquad (\text{if } \mu \ll \lambda\, \theta_1) \quad . \tag{4-3}$$

Solving for the parameters μ and λ between (4-1) and (4-3), we get

$$\lambda = \left(\frac{J}{b}\right)^{2/3} \quad \text{and} \quad \mu = \frac{4}{a^2}\left(\frac{b}{J}\right)^{4/3} \quad , \tag{4-4}$$

and a check on the requirement $\mu \ll \lambda\, \theta_1$ used above to ensure the validity of (4-1) and (4-3) implies

$$\theta_1 \gg \frac{4}{a^2}\frac{b^2}{J^2} \quad . \tag{4-5}$$

Making use of the inequality $\sin t \leqslant t$ for positive t, it is seen that

$$J(\theta_1) > \int_0^{\theta_1} \frac{dt}{t^{1/2}} = 2\theta_1^{1/2} \quad ,$$

THIS DOCUMENT PROVIDED BY THE ABBOTT AEROSPACE
TECHNICAL LIBRARY
ABBOTTAEROSPACE.COM

where $\frac{4b^2}{a^2 J^2} < \frac{b^2}{a^2 \theta_1}$ and the inequality (4-5) is certainly met if

$\theta_1 > \frac{b^2}{a^2 \theta_1}$, i.e. if $\theta_1 \gg b/a$, which is the regime under discussion in the present section.

Formulae (4-4) give λ and μ, whence $\rho(\theta)$ is known from (2-6) and the maximum value of the integral (2-1) is given by

$$I_m = J^{2/3} b^{1/3}$$

to this order of approximation. Since this expression increases with b, it follows that the maximum occurs when $b = b_m$, and

$$I_{max} = J^{2/3} b_m^{1/3} \quad . \tag{4-6}$$

Note that the region of validity discussed in this section and that of section 3 overlap when $b/a \ll \theta_1 \ll 1$, whence the results should be asymptotically equivalent. This is easily verified since in the limit $\theta_1 \gg b/a$ equation (3-6) takes the form

$$I_{max} \approx 2^{2/3} b^{1/3} \theta_1^{1/3} \qquad \text{for } \theta_1 \gg b/a \ ,$$

and agrees with (4-6) above, since for small θ_1, $J(\theta_1) \sim 2\theta_1^{1/2}$.

5 SPECIAL CASE $b/a \ll 1$, $\theta_1 = \pi/2$

As a special case of the results outlined in section 4, we give more detailed attention to the problem of optimising the integral I of (2-1) when $\theta_o = 0$ and $\theta_1 = \pi/2$. The parameters λ and μ are given approximately by (4-4), and their ratio

$$\delta^2 = \mu/\lambda \tag{5-1}$$

is small and of the order $(b/a)^2$. It is convenient to leave general values for λ and μ at this stage, and the analysis will recover the earlier results (4-4), together with slightly improved estimates.

In order to express the equation of the optimum curve in Cartesian form, we write

THIS DOCUMENT PROVIDED BY THE ABBOTT AEROSPACE TECHNICAL LIBRARY ABBOTTAEROSPACE.COM

$$x(t) = \int_0^t \rho \cos\theta \, dt \quad \text{and} \quad y(t) = \int_0^t \rho \sin\theta \, dt \quad , \qquad (5\text{-}2)$$

where $\rho^{-2/3} = (\mu \cos\theta + \lambda \sin\theta)$ and the parameters μ and λ are finally chosen so that $x(\pi/2) = a$ and $y(\pi/2) = b$.

The integral (5-2) for x can be performed explicitly, thus

$$x(t) = \int_0^t \frac{\cos\theta \, d\theta}{(\mu \cos\theta + \lambda \sin\theta)^{3/2}} = \frac{2}{\mu^{1/2}\lambda}\left\{1 - \frac{\mu^{1/2}}{(\mu \cos t + \lambda \sin t)^{1/2}}\right\} \quad ,$$

and since $\delta = (\mu/\lambda)^{1/2}$ is small, we have

$$x(t) \approx \frac{2}{\mu^{1/2}\lambda}\left\{1 - \frac{\delta}{(\delta^2 + \sin t)^{1/2}}\right\} \quad . \qquad (5\text{-}3)$$

To calculate the corresponding function $y(t)$, we have

$$y(t) = \int_0^t \frac{\sin\theta \, d\theta}{(\mu \cos\theta + \lambda \sin\theta)^{1/2}} \approx \int_0^t \frac{\sin\theta \, d\theta}{(\mu + \lambda \sin\theta)^{3/2}} \quad , \qquad (5\text{-}4)$$

since $\mu \cos\theta$ is negligible compared with $\lambda \sin\theta$, except near $\theta = 0$. The form of the function $y(t)$ is found to be different according as the parameter t is comparable with, or much greater than, the small number μ/λ.

(i) If $t \ll 1$, but t may be smaller or larger than μ/λ, then the trigonometrical functions of (5-4) may be simplified to get

$$y(t) = \frac{2\mu}{\lambda^{3/2}}\{2(1 + t/\delta^2)^{1/2} - (t/\delta^2)(1 + t/\delta^2)^{-1/2} - 2\} \quad .$$

If this is combined with (5-3), with $\sin t$ replaced by t for small t, the parameter may be eliminated to get

$$\frac{y}{(a_1 \delta^2)} = \frac{(x/a_1)^2}{1 - (x/a_1)} \qquad (5\text{-}5)$$

with $a_1 = 2/\lambda\mu^{1/2}$, and (5-5) is valid provided the angle $t \approx dy/dx$ is small, i.e. for $1 - x/a_1 \gg \delta$.

(ii) If $t \gg \mu/\lambda$, then we introduce an intermediate small number σ such that $t \gg \sigma \gg \mu/\lambda$, and subdivide the range of integration in (5-4) to get

THIS DOCUMENT PROVIDED BY THE ABBOTT AEROSPACE
TECHNICAL LIBRARY
ABBOTTAEROSPACE.COM

$$y(t) \approx \int_0^{\sigma} \frac{\theta\, d\theta}{(\mu + \lambda\theta)^{3/2}} + \int_{\sigma}^{t} \frac{\sin\theta\, d\theta}{(\lambda \sin\theta)^{3/2}} \approx \lambda^{-3/2} \int_0^{t} \frac{d\theta}{(\sin\theta)^{1/2}}$$

i.e.

$$y(t) \approx \lambda^{-3/2} J(t) \quad , \quad \text{where} \quad J(t) = \int_0^{t} \frac{d\theta}{(\sin\theta)^{1/2}} \quad . \tag{5-6}$$

In order to facilitate a numerical computation of the integral (5-6), it is convenient to remove the square root singularity by substituting $\sin\theta = s^2$, and by changing the parameter from t to $\tau = (\sin t)^{1/2}$. Thus

$$y(\tau) = \frac{2}{\lambda^{3/2}} F(\tau) \quad , \quad \text{where} \quad F(\tau) = \int_0^{\tau} \frac{ds}{(1 - s^4)^{1/2}} \quad , \quad 0 \leqslant \tau \leqslant 1 \quad . \tag{5-7}$$

The corresponding equation for $x(\tau)$ follows from (5-3) whence

$$x(\tau) = \frac{2}{\mu^{1/2}\ \lambda} (1 - \delta/\tau) \quad . \tag{5-8}$$

The function $F(\tau)$ can be computed numerically, and a graph thereof is presented in Fig.5; it is readily found from its definition (5-7) that

$$F(\tau) \sim \tau \qquad \text{for small} \quad \tau \quad . \tag{5-9}$$

Thus the curve S is given by (5-5) for $1 - x/a_1 \gg \delta$, and by (5-7), (5-8) for $1 - x/a_1 \ll 1$; the two representations are readily shown to be asymptotically equivalent in their common region $\delta \ll 1 - x/a_1 \ll 1$.

The constants λ and μ have to be chosen so that $x = a$ and $y = b$ at the end point $\tau = 1$. Thus if $F(1)$ is written as F_1, (5-7) and (5-8) imply

$$b = \frac{2F_1}{\lambda^{3/2}} \quad \text{and} \quad a = \frac{2}{\mu^{1/2}\ \lambda} (1 - \mu^{1/2}/\lambda^{1/2}) \quad ,$$

whose solution for small μ/λ (i.e. small b/a) is given as

$$\lambda^{3/2} = \frac{2F_1}{b} \quad \text{and} \quad \mu^{1/2} = \left(\frac{2F_1}{b}\right)^{1/3} \left(\frac{b}{aF_1} - \frac{b^2}{a^2F_1^2}\right) \quad . \tag{5-10}$$

If only the leading term of (5-10) is retained, with $b^2/a^2F_1^2$ neglected, then we recover an earlier result (4-4). The higher order term is retained here, since otherwise the end point of the curve, obtained by setting $\tau = 1$ in (5-7), (5-8), would be situated at

THIS DOCUMENT PROVIDED BY THE ABBOTT AEROSPACE
TECHNICAL LIBRARY
ABBOTTAEROSPACE.COM

$$y = b \quad \text{and} \quad x = a(1 - b/a) \quad ;$$

although this is correct to our first order approximation for small b/a, it has an unacceptable error in the x-coordinate for finite values of b/a.

With the values (5-10) for λ and μ, the associated constants δ and a_1 are given by

$$\delta = \frac{b}{aF_1} - \frac{b^2}{a^2F_1^2} \approx \frac{b}{aF_1} \quad \text{and} \quad a_1 = a + \frac{b}{F_1} \quad . \tag{5-11}$$

The curve S is then given by

$$\frac{y}{a_1\delta^2} = \frac{(x/a_1)^2}{1 - (x/a_1)} \quad , \quad \text{for} \quad 1 - (x/a_1) \gg \delta \tag{5-12}$$

and by

$$x(\tau) \approx a_1 \, (1 - \delta/\tau) \; , \quad y(\tau) = b \, F(\tau)/F(1) \quad , \quad \text{for} \quad 1 - (x/a_1) \ll 1, \tag{5-13}$$

where $F(\tau)$ is given by (5-7) and is sketched in Fig.5.

Note that the value of x at the end point $\tau = 1$ is given by

$$x(1) = \left(a + \frac{b}{F_1}\right)\left(1 - \frac{b}{aF_1}\right) = a + O(b/a)^2 \quad ,$$

and is much closer to its correct value than that, $x = a + O(b/a)$, obtained by retaining only the leading term of (5-10).

A sketch of the curve S is shown in Fig.4, for particular values of the parameters a and b.

According to the general theory of section 2, the curve S described above is such that the value of the integral

$$I(\theta) = \int_0^\theta \rho^{1/3} \, d\theta$$

is optimised when θ takes the value $\pi/2$, when I takes the value

$$I(\pi/2) = \mu a + \lambda b \approx \left(\frac{2F_1}{b}\right)^{2/3} b \quad . \tag{5-14}$$

THIS DOCUMENT PROVIDED BY THE ABBOTT AEROSPACE
TECHNICAL LIBRARY
ABBOTTAEROSPACE.COM

It is of interest to evaluate the integral I at intermediate values of θ, in order to compare with the corresponding function (3-7). We have

$$I(\theta) = \int_0^\theta \frac{dt}{(\mu \cos t + \lambda \sin t)^{1/2}} \approx \int_0^\theta \frac{dt}{(\mu + \lambda \sin t)^{1/2}} , \qquad (5\text{-}15)$$

and the character of the integral is different according as θ is comparable with, or much larger than, the small parameter $\delta^2 = \mu/\lambda$.

(i) If $\theta \ll 1$, but may be large or small compared with δ^2, then the sine function of (5-15) may be replaced by t, to get

$$I(\theta) \approx \frac{2}{\lambda} \{(\mu + \lambda\theta)^{1/2} - \mu^{1/2}\}$$

i.e.

$$I \approx 2\left(\frac{2F_1}{b}\right)^{-1/3} \{(\theta + \delta^2)^{1/2} - \delta\} \qquad \text{for } \theta \ll 1 , \qquad (5\text{-}16)$$

where $\delta \approx b/aF_1$.

(ii) If $\theta \gg \delta$, then we introduce a small parameter σ such that $\theta \gg \sigma \gg \delta$; whence

$$I \approx \int_0^\sigma \frac{dt}{(\mu + \lambda t)^{1/2}} + \int_\sigma^\theta \frac{dt}{(\lambda \sin t)^{1/2}} \approx \lambda^{-1/2} \int_0^\theta \frac{dt}{(\sin t)^{1/2}}$$

i.e.

$$I \approx 2\left(\frac{2F_1}{b}\right)^{-1/3} F((\sin \theta)^{1/2}) \qquad \text{for } \theta \gg \delta \qquad (5\text{-}17)$$

The two approximations (5-16), (5-17) are asymptotically equivalent in their common region of validity $\delta \ll \theta \ll 1$, and together provide information regarding I for all values of θ from 0 to $\pi/2$. A sketch is shown on Fig.2, with special values for a, b.

6 CONCLUSION

The integral $I(\theta) = \int_0^\theta \rho^{1/3}(\theta')\, d\theta'$ can be maximised for a given value $\theta = \theta_1$ by choosing a suitable path with end points at $(0,0)$ and (a,b), where a is fixed and b has to be not greater than a fixed value b_m. Thus for any given direction θ_1 at the end point an optimum curve is defined,

THIS DOCUMENT PROVIDED BY THE ABBOTT AEROSPACE
TECHNICAL LIBRARY
ABBOTTAEROSPACE.COM

whence the largest possible value $I_{max}(\theta_1)$ is found. Since a different curve S is appropriate for each chosen value of θ_1 it follows that the value of $I(\theta)$, evaluated on a curve chosen to maximise $I(\theta_1)$ takes its optimum value when $\theta = \theta_1$, with $I(\theta) \leqslant I_{max}(\theta)$ for all other angles $\theta \neq \theta_1$. The general shape of $I_{max}(\theta)$ is shown on Fig.2, and a more specific graph is drawn on Fig.3, with definite values for a and b_m.

General results are given in the text for any θ_1, b and a, subject to the limiting assumption $b/a \ll 1$. Particular attention is directed to three cases:

(a) curve S chosen to optimise $I(\theta_1)$, with θ_1 small

(b) curve S chosen to optimise $I(\theta_1)$, with $\theta_1 = 2b_m/a$

(c) curve S chosen to optimise $I(\theta_1)$, with $\theta_1 = \pi/2$.

The functions $I(\theta)$ are shown in Fig.3 for each of these cases, with the corresponding curves S sketched in Fig.4. It is seen that for $\theta_1 \leqslant 2b_m/a$, the curve that maximises $I(\theta_1)$ is simply a circular arc with end points at (0,0) and $(a, \frac{1}{2}a\theta_1)$.

The 'best' curve is such that $I(\theta)$ is close to $I_{max}(\theta)$ for as large a range of values of θ as possible, with particular weight given to smaller values of θ, since it is desired to produce a high value of $I(\theta)$ as soon as possible with increasing θ. Of the two cases (b) and (c) shown in Fig.3, it is seen that $I_{(b)}$ exceeds $I_{(c)}$ for values of θ between about 1/5 and 2/5 radians, with $I_{(c)}$ greater than $I_{(b)}$ for other values of θ.

Finally, it should be remarked that the curves for case (c) on Figs.3 and 4, give a qualitative, rather than quantitatively accurate, picture of the precise shapes. Each of these curves is specified by a pair of formulae (5-16), (5-17) and (5-12), (5-13) that match to form smooth curves in the asymptotic limit $b/a \to 0$; they do not, of course, match perfectly when b/a is finite, and $b/a = 1/6$ in the illustrative examples. The correct curves can be calculated numerically, using (5-13) and (5-3), (5-4), with λ and μ given by (5-10).

THIS DOCUMENT PROVIDED BY THE ABBOTT AEROSPACE
TECHNICAL LIBRARY
ABBOTTAEROSPACE.COM

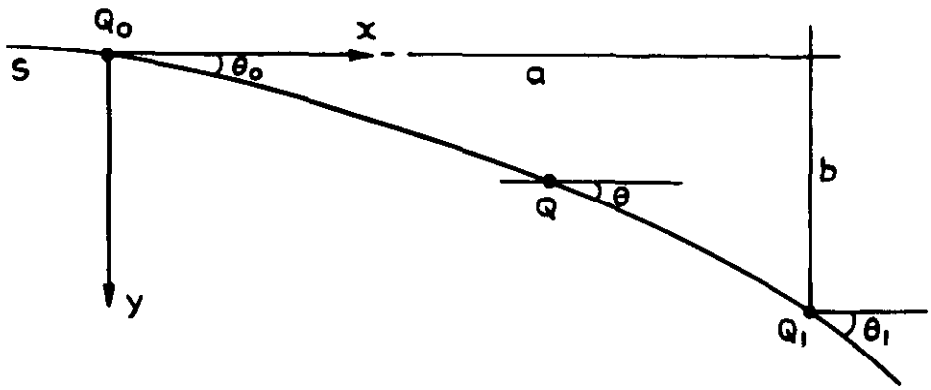

Q_o and Q_1 are fixed points and the curve S has tangents with angles θ_o and θ_1 to the horizontal

Fig.1 Coordinate system

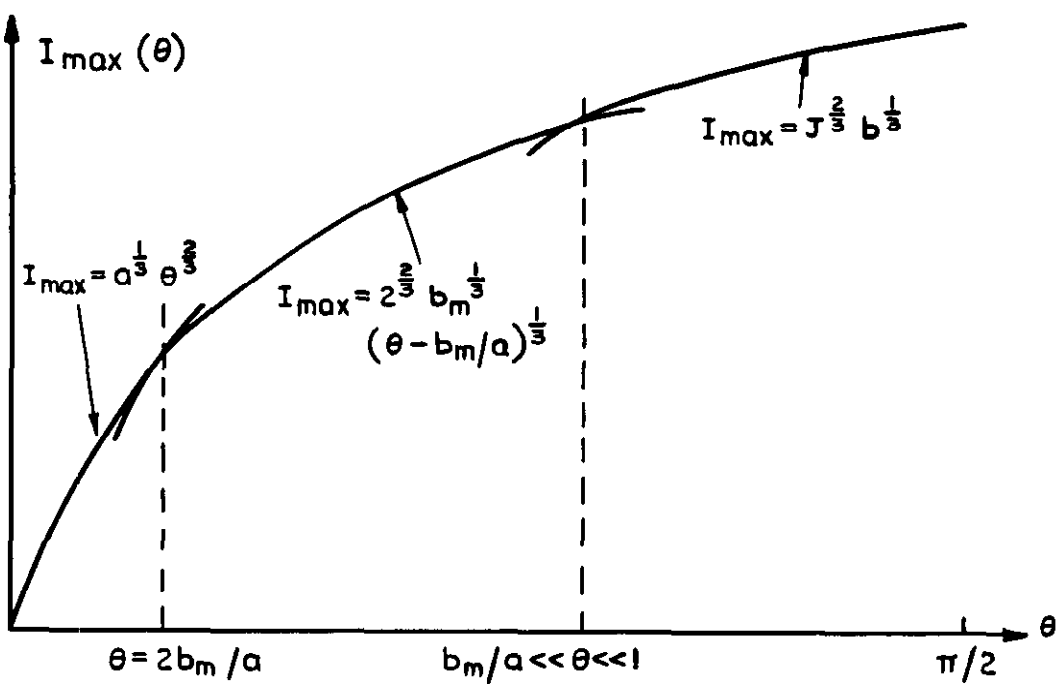

Fig.2 $I_{max}(\theta)$ against θ, showing the three different regions

THIS DOCUMENT PROVIDED BY THE ABBOTT AEROSPACE
TECHNICAL LIBRARY
ABBOTTAEROSPACE.COM

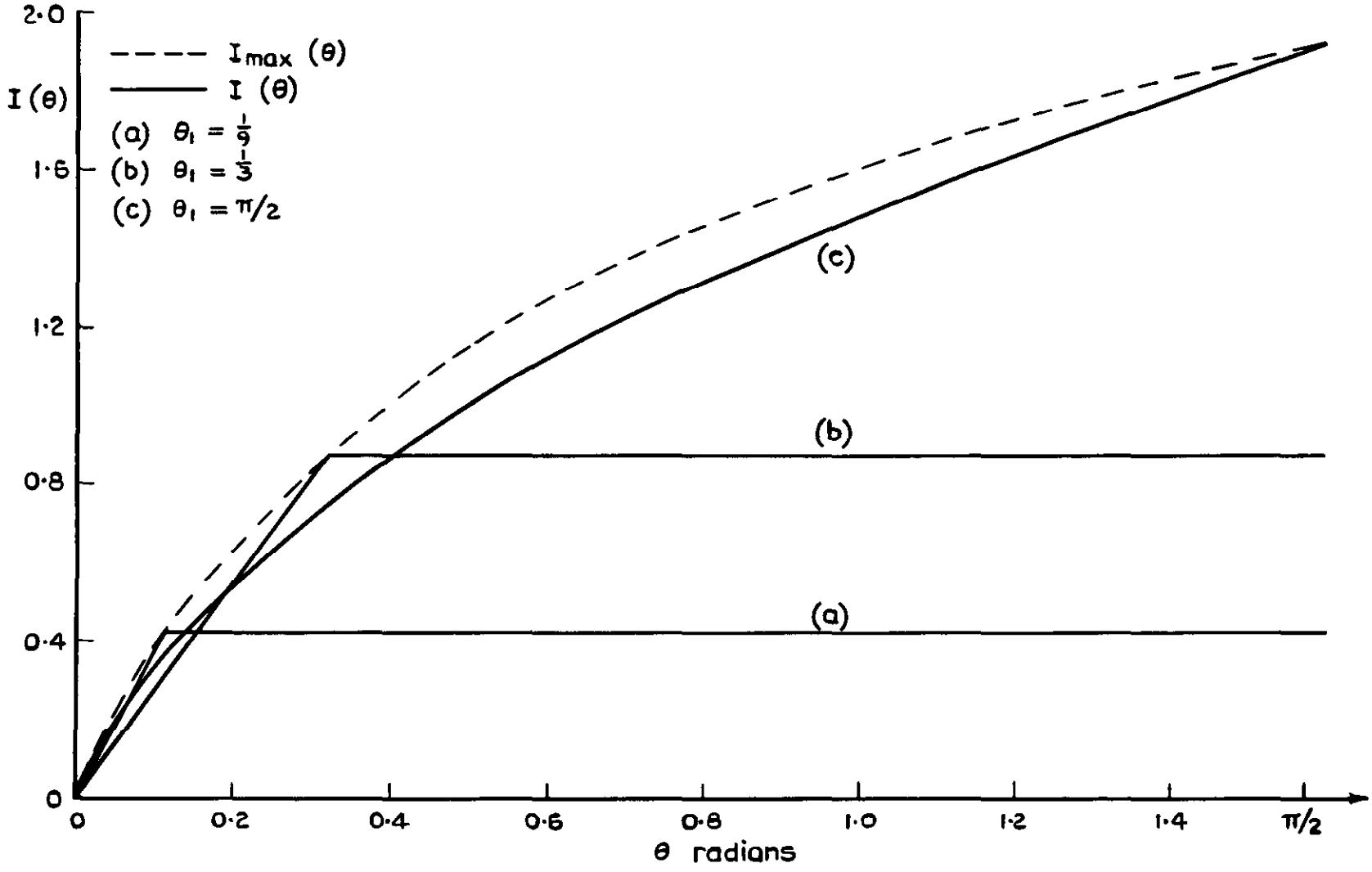

Fig.3 Integral I(θ) as a function of θ

THIS DOCUMENT PROVIDED BY THE ABBOTT AEROSPACE
TECHNICAL LIBRARY
ABBOTTAEROSPACE.COM

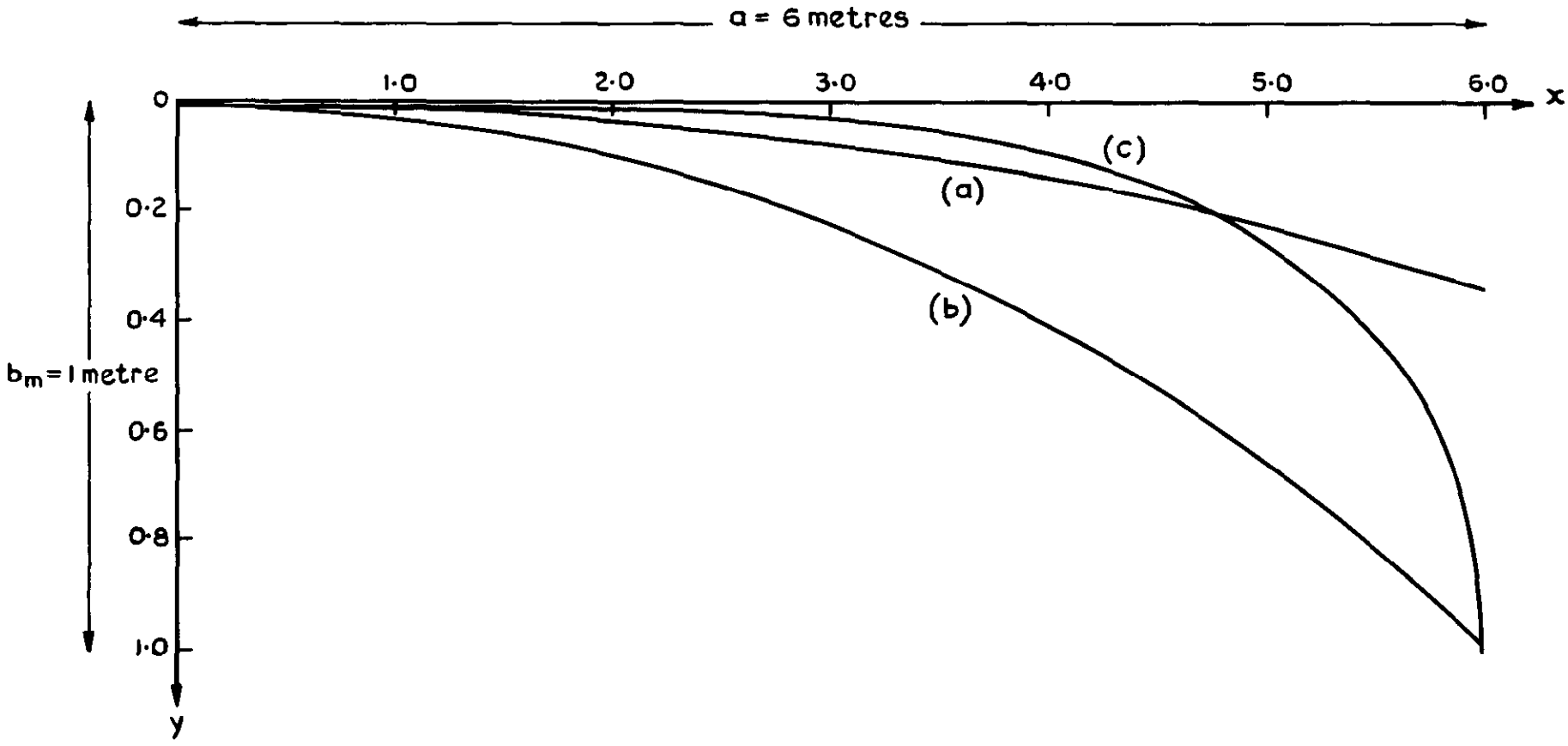

Fig.4 Optimum curves in cases (a) $\theta_1 = \frac{1}{9}$, (b) $\theta_1 = \frac{1}{3}$, and (c) $\theta_1 = \pi/2$

THIS DOCUMENT PROVIDED BY THE ABBOTT AEROSPACE
TECHNICAL LIBRARY
ABBOTTAEROSPACE.COM

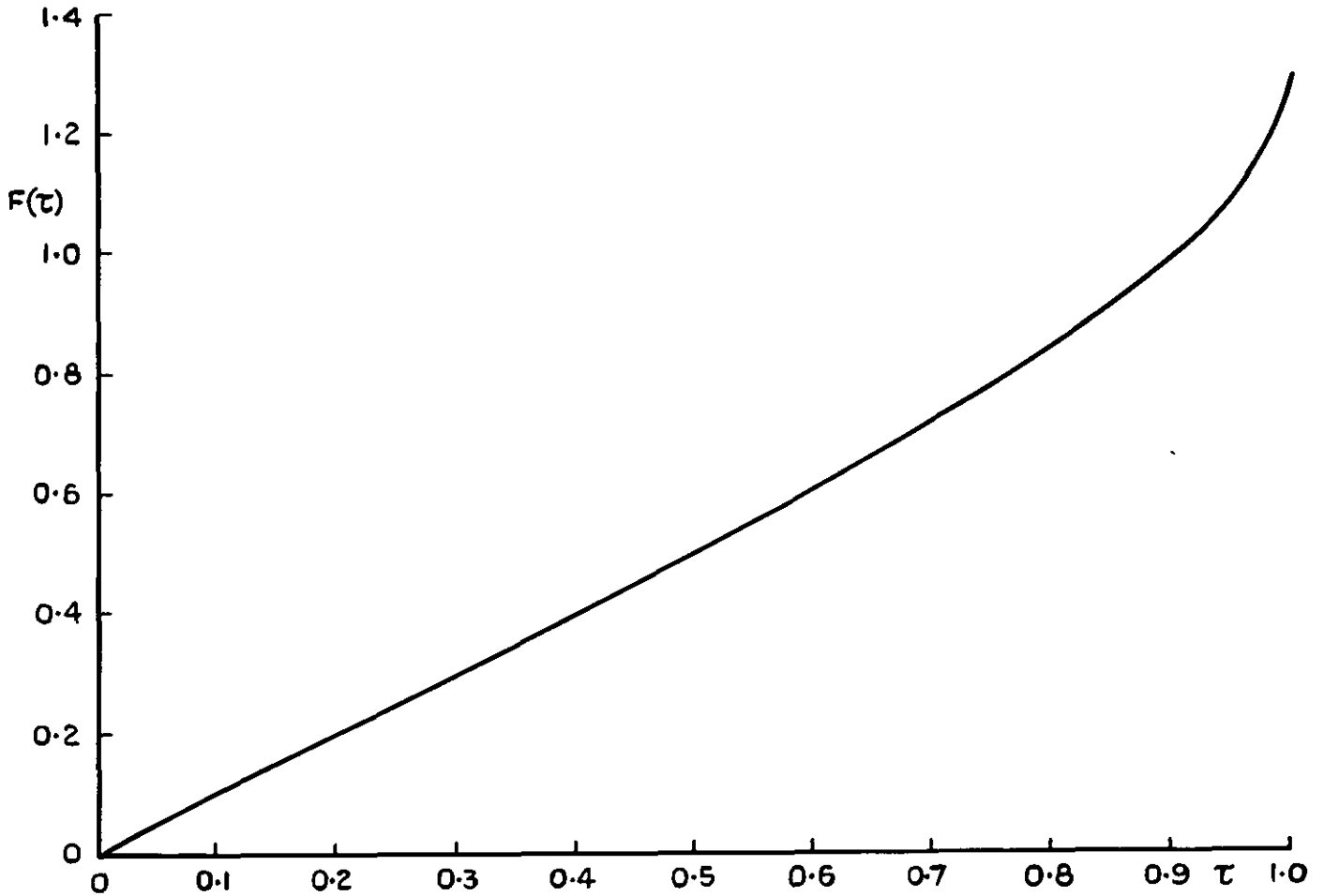

Fig. 5 The function $F(\tau) = \int_0^{\tau} \frac{ds}{(1-s^4)^{1/2}}$

Printed in England for Her Majesty's Stationery Office by the Royal Aircraft Establishment, Farnborough. Dd 502109 K 4

THIS DOCUMENT PROVIDED BY THE ABBOTT AEROSPACE
TECHNICAL LIBRARY
ABBOTTAEROSPACE.COM

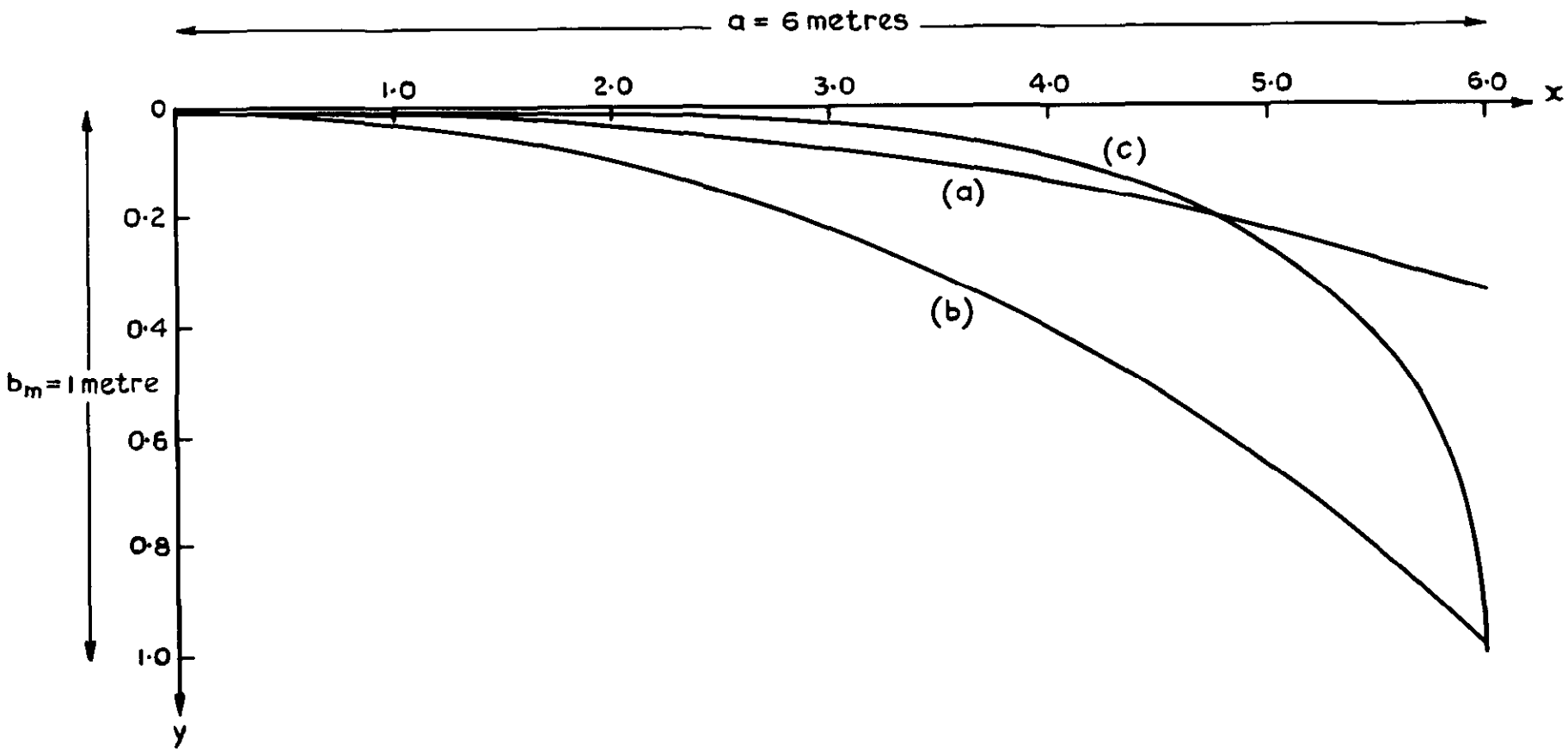

Fig.4 Optimum curves in cases (a) $\theta_1 = \frac{1}{9}$, (b) $\theta_1 = \frac{1}{3}$, and (c) $\theta_1 = \frac{\pi}{2}$

THIS DOCUMENT PROVIDED BY THE ABBOTT AEROSPACE
TECHNICAL LIBRARY
ABBOTTAEROSPACE.COM

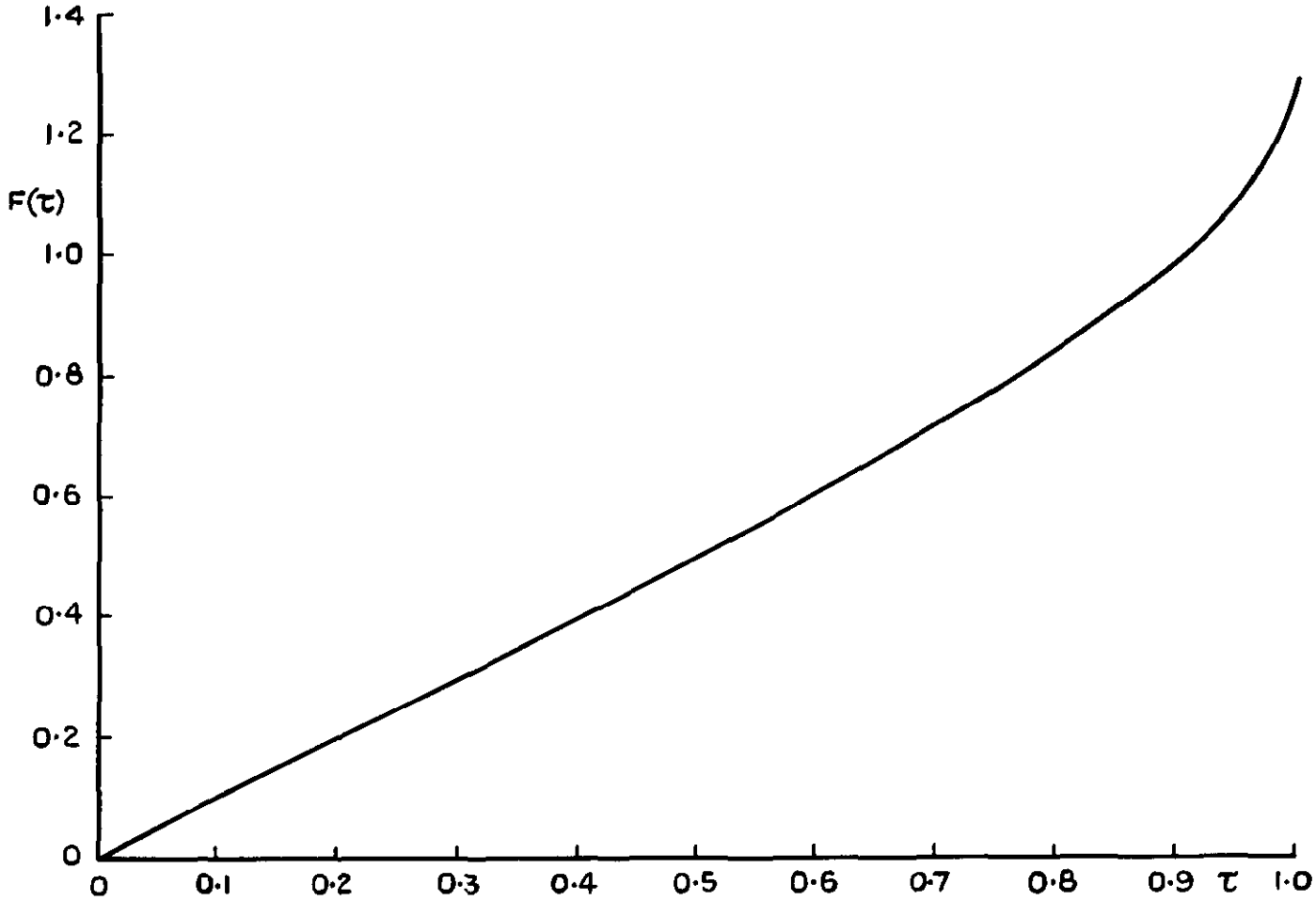

Fig. 5 The function $F(\tau) = \int_0^{\tau} \frac{ds}{(1-s^4)^{1/2}}$

Printed in England for Her Majesty's Stationery Office by the Royal Aircraft Establishment, Farnborough. Dd 502109 K 4

THIS DOCUMENT PROVIDED BY THE ABBOTT AEROSPACE
TECHNICAL LIBRARY
ABBOTTAEROSPACE.COM

DETACHABLE ABSTRACT CARD

A.R.C C.P. No 1193
October 1970

534.26
534-8

Leppington, F G

CURVATURE EFFECTS IN THE DIFFRACTION OF SHORT WAVES INTO A SHADOW

PART A

The distant pressure field within the shadow cast by a point source in the presence of a semi-infinite rigid plane is compared with that for a rounded body Within the 'deep shadow region', not too close to the shadow boundary, it is found that the field is much less for the rounded obstacle in the short wave limit, having exponentially small behaviour compared with the algebraic decay appropriate to the half-plane case At points very close to the geometrical shadow boundary, on the other hand, the pressure field exhibits almost identical behaviour for each geometry, this being the familiar Fresnel pattern, but with a change of phase for the rounded body

PART B

Consideration is given to the possibility of choosing the shape of a rounded obstacle, within certain overall restrictions, in order to minimise the diffracted field within the deep shadow region

A.R C C.P No 1193
October 1970

534.26
534-8

Leppington, F G

CURVATURE EFFECTS IN THE DIFFRACTION OF SHORT WAVES INTO A SHADOW

PART A

The distant pressure field within the shadow cast by a point source in the presence of a semi-infinite rigid plane is compared with that for a rounded body. Within the 'deep shadow region', not too close to the shadow boundary, it is found that the field is much less for the rounded obstacle in the short wave limit, having exponentially small behaviour compared with the algebraic decay appropriate to the half-plane case. At points very close to the geometrical shadow boundary, on the other hand, the pressure field exhibits almost identical behaviour for each geometry, this being the familiar Fresnel pattern, but with a change of phase for the rounded body.

PART B

Consideration is given to the possibility of choosing the shape of a rounded obstacle, within certain overall restrictions, in order to minimise the diffracted field within the deep shadow region

This Document Provided by the Abbott Aerospace
Technical Library
abbottaerospace.com

This Document Provided by the ABBOTT AEROSPACE
TECHNICAL LIBRARY
ABBOTTAEROSPACE.COM

This Document Provided by the Abbott Aerospace
TECHNICAL LIBRARY
ABBOTTAEROSPACE.COM

© *Crown copyright 1971*

Published by
HER MAJESTY'S STATIONERY OFFICE

To be purchased from
49 High Holborn, London WC1 V 6HB
13a Castle Street, Edinburgh EH2 3AR
109 St Mary Street, Cardiff CF1 1JW
Brazennose Street, Manchester M60 8AS
50 Fairfax Street, Bristol BS1 3DE
258 Broad Street, Birmingham B1 2HE
80 Chichester Street, Belfast BT1 4JY
or through booksellers

C.P. No. 1193

SBN 11 470461 9